PHILOSOPHICAL TRANSACTIONS OF THE ROYAL SOCIETY B BIOLOGICAL SCIENCES

Dissipative Structures and Morphogenetic Pattern in Unicellular Algae

T. C. Lacalli

Phil. Trans. R. Soc. Lond. B 1981 **294**, 547-588
doi: 10.1098/rstb.1981.0118

Phil. Trans. R. Soc. Lond. B **294**, 547–588 (1981) [547]
Printed in Great Britain

DISSIPATIVE STRUCTURES AND MORPHOGENETIC PATTERN IN UNICELLULAR ALGAE

By T. C. LACALLI
Biology Department, University of Saskatchewan, Saskatoon, Canada S7N 0W0

(*Communicated by J. Heslop-Harrison, F.R.S. – Received* 11 *November* 1980)

CONTENTS

Patterns of cell wall growth and ornamentation in unicellular algae, mainly in desmids, are compared with patterns generated by Tyson's Brusselator, a two-morphogen reaction–diffusion model. The model generates hexagonal arrays of points in two dimensions, according well with the observed patterns of surface ornamentation on desmid zygospores. Computed patterns in one dimension and of branching on a circular disc account both qualitatively and quantitatively for morphogenetic patterns that develop following cell division in several desmid genera. Cell wall ingrowths appear to be under similar pattern control to wall outgrowths during morphogenesis, which suggests the involvement of a reaction–diffusion mechanism in establishing and correctly positioning the cell division septum. The application of the model to morphogenesis in *Acetabularia* and diatoms is also discussed.

1. Introduction

An initially homogeneous chemical system can develop standing concentration waves if appropriate reactions occur involving autocatalytic and cross-catalytic interactions between two chemical species diffusing within the system. Since the appearance of Turing's description and

analysis of this phenomenon (Turing 1952), and because of increasing interest in the general class of dissipative structures of which Turing's model is one example (Glansdorff & Prigogine 1973), biologists have sought to identify patterns in living organisms that might have arisen as a consequence of a reaction–diffusion mechanism. Their strategy has been to compare patterns found in living organisms with the predictions of the linear equations discussed by Turing or of various specific nonlinear models. The most convincing comparisons have been those involving either a complex pattern or a number of related variants of one pattern, since greater demands are thereby placed on the predictive power of the theory. For example, a remarkable correspondence can be shown between the predicted patterns of wave harmonics on an ellipse and the succession of compartment boundaries that appear on the roughly elliptical imaginal wing disc of *Drosophila* during its development (Kauffman *et al.* 1978). In this example, pattern develops in an epithelial sheet of many cells. The catalytic reactions presumably occur within the cells, each cell acting as a well stirred unit of the system, while diffusion is responsible for the transport of material between cells.

The suggestion that a reaction–diffusion mechanism might account for the patterns of morphogenesis in unicellular algae was first made by Wardlaw (1953, 1955), but this suggestion has not been explored in any detail. The patterns most likely to be of interest have not been catalogued in an organized fashion, and there has been no analysis of specific reaction–diffusion mechanisms regarding their suitability as models for algal morphogenesis. The present paper is intended to remedy this oversight, with emphasis on morphogenesis in the group of freshwater green algae known as desmids. In the examples to be considered, pattern is ultimately expressed in the shape of the developing cell wall or, in the case of diatoms, of the siliceous frustule. By and large, in these examples, careful examination has as yet failed to reveal an ordering of the cell cytoplasm or of the cytoplasmic organelles that corresponds in any obvious way with the developing pattern during the early stages of morphogenesis. Further, in many cases, the continuous agitation of the cytoplasm by means of cytoplasmic streaming makes the conveyance of pattern information through the cytoplasm seem unlikely. The supposition is therefore made that pattern is generated at or near the surface of the cell. The system in which chemical reactions and diffusion operate to accomplish this is taken to be two-dimensional, involving one or more of (1) the cell membrane, (2) the approximately two-dimensional space occupied by the cell wall and (3) the thin layer of cytoplasm lying immediately under the cell membrane and excluded from the active streaming.

This survey of algal pattern is an extension of an earlier analysis of the pattern of pores found in desmid cell walls (Lacalli & Harrison 1978*b*). Patterns approximating the observed pattern of pores can be produced by supposing that pores are initiated randomly over the surface of the cell with initiation followed by the rapid development of an area of inhibition around each within which no additional pores can become established. The degree of order that can be achieved by such a mechanism is strictly limited and, as described below (§2), examples of surface pattern are known in plant cells that are clearly too ordered to have been generated by this means. The mechanism responsible for such patterns must therefore involve initiation steps that are spatially more ordered than a random distribution of points. A reaction–diffusion mechanism is one means of imposing a spatial periodicity on the initiation step, although it is by no means the only way. Surface pattern in single cells nevertheless represents an attractive system for testing the applicability of reaction–diffusion models to morphogenesis. It is reasonable, at least initially, to assume that relatively straightforward sequences of reactions localized

near the cell surface are responsible for the catalytic formation and destruction of the relevant morphogenetic substances, with diffusion being the principal means of their transport in the plane of the cell membrane and cell wall. Multicellular systems are potentially much more complex. The entire synthetic and metabolic machinery of the cell is available to generate an overall auto- or cross-catalytic effect on the formation and destruction of morphogenetic substances, and there are a number of ways, besides diffusion, for these to be transported between cells.

The types of patterns to be expected of reaction–diffusion mechanisms have been discussed in general terms by Gmitro & Scriven (1966) based on solutions to linear equations. For a particular nonlinear model, some patterns will be quite similar to the predicted linear patterns while others, if highly dependent on the nonlinearities, may be substantially different. One-dimensional patterns tend to fall within the former category: when the intrinsic pattern wavelength is small relative to system size a row of identical sine waves is generated in the linear case, and, though the waveform may be altered, a simple one-dimensional periodicity is also characteristic of the nonlinear models that have been studied (see, for example, Herschkowitz-Kaufman 1975). For a wavelength roughly comparable to system size, a harmonic pattern fitting the boundary conditions of the system is generated in both linear and, with some modification, nonlinear cases (see, for example, Erneux & Herschkowitz-Kaufman 1975). Other patterns and, in particular, pattern changes in response to changing parameters or boundary conditions, appear to depend crucially on the nonlinear part of the governing equations. For example, the nonlinearities determine whether a simple, one-dimensional periodicity translates in two dimensions into a square array, a hexagonal array or some other pattern (§3).

The model used throughout this paper, discussed in detail in §3, was developed by Tyson and coworkers (Tyson & Light 1973; Tyson & Kauffman 1975). It is a variant of the 'Brusselator' model which has been subjected to extensive analytical treatment (Herschkowitz-Kaufman 1975; Erneux & Herschkowitz-Kaufman 1979*a*, *b*; Kubicek *et al.* 1978). Tyson's Brusselator has the important feature that the morphogen peaks, once established, are capable of movement in response to changes to the system boundaries. Further, in response to an increase in system size, a single peak can branch and produce additional peaks or other patterns. Whereas some morphogenetic models depend for their usefulness on their inability to respond in this way (e.g. the model proposed by Gierer & Meinhardt (1972)), the utility of Tyson's Brusselator with regard to algal morphogenesis is dependent on these behaviours, both because of the branching in itself and because, in two dimensions, hexagonal arrays of points can be generated by means of branching and movement of peaks.

Four basic pattern types are considered in the sections that follow: periodic arrays in one and in two dimensions, harmonic fitting of simple waveforms (single peaks) to boundary conditions, and generation of new patterns from the latter by branching. A number of variations on these basic types occur in the algal examples discussed. Two-dimensional arrays and dichotomous and more complex forms of branching are particularly well illustrated by desmids (§4), and desmids therefore figure prominently in the comparison of theory with observed cell patterns. Patterns of zygospore ornamentation in desmids, essentially hexagonal arrays, accord extremely well with the two-dimensional patterns generated by the model. There is also good agreement between computed patterns and patterns of semicell morphogenesis in desmids, though with some unsatisfactory features. The appropriate computations do not specify pattern unequivocally. Instead, they define a range of possible pattern behaviour, and not all features

PHILOSOPHICAL TRANSACTIONS OF THE ROYAL SOCIETY B BIOLOGICAL SCIENCES

of semicell morphogenesis can be accommodated, even within this range. Nevertheless, significant morphogenetic problems are potentially resolvable on the basis of reaction–diffusion theory. Evidence from desmids suggests that both cell wall ingrowths and cell wall outgrowths may be under the control of a single patterning mechanism and, further, that a reaction–diffusion mechanism may be involved in specifying the plane of cell division. The computational results are also compared with patterns in *Acetabularia* (§5) and diatoms (§6) with, in §7, suggestions regarding possible experimental tests of the theory.

2. Measuring order: an example with too much order

Since patterns of points on a two-dimensional surface and along a line are frequently referred to in this paper, it is important to have some means of quantifying their degree of order to allow comparison between them. The means adopted here is that of the Clark & Evans R parameter, whose use for analysis of two-dimensional pattern (R_2 for two dimensions) has been previously discussed in some detail (Lacalli & Harrison 1978*b*). A one-dimensional analogue, R_1, is also employed.

The R parameter is the ratio between the mean of observed distances between each pattern point, taken in turn, and its nearest neighbour ($\bar{r}_a$) to that expected for a random distribution of points ($\bar{r}_e$). In two dimensions, $\bar{r}_e = \frac{1}{2}\rho^{-\frac{1}{2}}$, where ρ is the area density of pattern points. For a perfect hexagonal array $R_2 = 2.1491$ and for a perfect square array $R_2 = 2$ exactly. Decrease of R_2 below these values indicates either a loss of order ($R_2 = 1$ for randomness) or a change from regular to clustered order. The latter is assumed to be absent in the examples to be discussed.

The generation of two-dimensional patterns through an inhibitory field mechanism has already been mentioned as a model for pore formation in desmids. Pattern points are initiated randomly, and are surrounded by inhibitory fields within which no further points can form. Claxton (1964) constructed examples of such patterns by hand and, for inhibitory fields of fixed size, obtained values of R_2 of 1.757 ± 0.005 (three trials). The observed order of pores is somewhat below this value, consistent with the lesser degree of order to be expected for inhibitory fields with a time-dependent radius. The latter is more easily justifiable in chemical terms than the constant-radius inhibitory field.

For a pattern of points in one dimension, $\bar{r}_e = 1/2\rho$ (Hertz 1909). The maximum value of R_1 is then 2. From computer-generated inhibitory field patterns for quite large one-dimensional systems, using the time-independent inhibitory field, the present author obtained values for R_1 of 1.783 ± 0.004 (18 trials) as a one-dimensional analogue of Claxton's calculation.

Biological patterns that exceed the above R values for inhibitory field models are worthy of special attention because, to account for such patterns, it becomes necessary to invoke mechanisms with greater than random ordering capability in the initiation step. It is important to show that such patterns exist, since they are likely candidates for comparison with the patterns generated by reaction–diffusion models.

The best documented such pattern for a unicellular plant system is the nearly perfect hexagonal array of spines ($R_2 = 2.08$) on the surface of developing *Tagetes* pollen grains. Heslop-Harrison (1969) has followed the development of this pattern from the first appearance of small papillae, representing projections from the cell wall surface of groups of structures known as probacula, to the final stage in which most of the original space between adjacent papillae is

obliterated by the growth of the papillae to form large spines. The hexagonal pattern is most clearly shown in the early stages. Development of some surface features on pollen grains appears to involve spatial ordering of the underlying cytoplasm. The grain apertures, for example, form at points where cisternae of endoplasmic reticulum become closely applied to the cell membrane (Heslop-Harrison 1968, 1972). A similar association of cytoplasmic membranes is seen adjacent to developing probacula in some species, but the appropriate stages in *Tagetes* have yet to be investigated in this regard. Regardless of whether such patterns are first generated at the cell surface or deeper within the cytoplasm, the origin of hexagonal order is still unexplained. Considering the small size of the papillae (radius ≈ 0.2 μm) compared with the distance between papillae (*ca.* 2 μm from figure 1 of Heslop-Harrison 1969), it seems unlikely that the pattern is simply a consequence of close packing of some larger structural element. An inhibitory field mechanism, at least in its simplest version with random initiation, is clearly an inadequate explanation for the pattern, and one must search instead for mechanisms that generate substantially more order in the first instance.

3. Computed wave patterns: Tyson's Brusselator

The model used throughout this paper for generating patterns was developed by Tyson and coworkers (Tyson & Light 1973; Tyson & Kauffman 1975) principally as a model for studying time-oscillatory phenomena. The mechanism involves formation and destruction of two morphogens, X and Y, with rate constants *a*–*d*, as follows:

$$\begin{aligned} \text{reactants} &\xrightarrow{a} \mathrm{Y}, \\ \mathrm{Y} &\xrightarrow{b} \mathrm{X}, \\ \mathrm{Y}+2\mathrm{X} &\xrightarrow{c} 3\mathrm{X}, \\ \mathrm{X} &\xrightarrow{d} \text{products}. \end{aligned}$$

The rate equations, including diffusion, with concentration variables X and Y and diffusivities $\mathscr{D}_X$ and $\mathscr{D}_Y$, are:

$$\left.\begin{aligned} \partial X/\partial t &= bY + cX^2Y - dX + \mathscr{D}_X\nabla^2 X, \\ \partial Y/\partial t &= a - bY - cX^2Y + \mathscr{D}_Y\nabla^2 Y. \end{aligned}\right\} \quad (1)$$

For different choices of parameter values, the model can generate a variety of behaviours, which include spatially uniform limit cycle oscillations around the steady state, stable spatial waves or oscillating spatial waves. A simple analysis of the conditions on parameters required to produce these various behaviours is given by Lacalli & Harrison (1979). For a one-dimensional system, the spatial part of the solution of the linearized form of equations (1) is in the form of sine waves, with waves of different wavelength, each with a characteristic exponential growth rate. Spatial pattern depends upon having a maximum in the curve relating growth rate (k_g) and wavelength (λ) at some finite wavelength (λ_m). There is a critical length (l_0) below which no pattern will develop. For a system longer than l_0, a pattern will develop with pattern wavelength as close to λ_m as the boundary conditions permit. Formulae for calculating k_g, λ_m and l_0 can be found in the previous papers in this series (Lacalli & Harrison 1978*a*, 1979).

The patterns and pattern changes figured in this section have all been carried out as explicit, finite-difference calculations based on equations (1) except for the example shown in figure 9*b*, which is for the Gierer & Meinhardt model. Because of the conditions on diffusivities, that X

must be the more slowly diffusing of the two morphogens, concentration peaks are much sharper for X than for Y. The figures show X concentration only except figure 1*c*, *d* which also show Y. The concentration profile for Y is in all cases out of phase with X and much shallower. In calculations showing the effect on pattern of growth in system size, the actual size of the system has been kept the same for ease of computation while its effective size, relative to λ_m, is increased by reducing λ_m through change of rate constants and diffusivities.

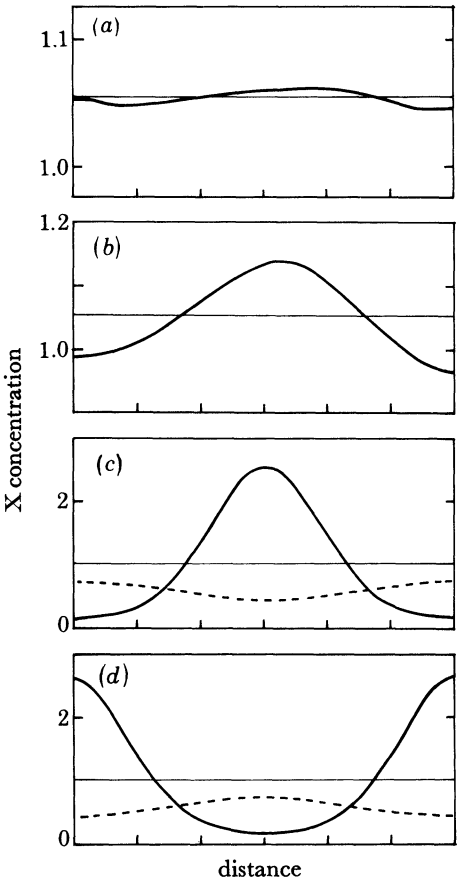

FIGURE 1. Generation of ternary pattern from initial steady state (solid line) and random disturbances. X concentration (solid curve) is shown at (*a*) 4000, (*b*) 8000 and (*c*) 16000 iterations. (*d*) Reverse ternary pattern generated in the same way. Y concentration is shown as a dotted curve in (*c*) and (*d*). Details of this and other computations are given in §8.1.

In choosing a simple nonlinear model such as Tyson's, undoubtedly much of the richness of pattern behaviour of more complex models is lost. Tyson's model does, however, produce a variety of patterns whose development, even if simple, is as yet incompletely understood. An analysis of these is a logical first step in exploring the behaviour of more complex models and, in addition, the more complex models are quite likely to be homomorphic under many conditions. That is, they will be characterized by patterns and pattern changes that are either identical or fundamentally related.

PHILOSOPHICAL TRANSACTIONS OF THE ROYAL SOCIETY B BIOLOGICAL SCIENCES

3.1. *Pattern in one dimension*

Beginning with steady state values of X and Y, introduction of random concentration fluctuations in a one-dimensional system of appropriate length ($l \approx \lambda_m$) with zero-flux boundary conditions will generate a single wave with central maximum of X, as shown in figure 1*a–c*, or its reverse, with a central minimum (figure 1*d*). The single wave pattern will be referred to here as ternary pattern because there are three regions over which deviations from the steady state give either maxima or minima in concentration. The half-wave pattern with two such regions (e.g. figure 6*a*) is then a binary pattern.

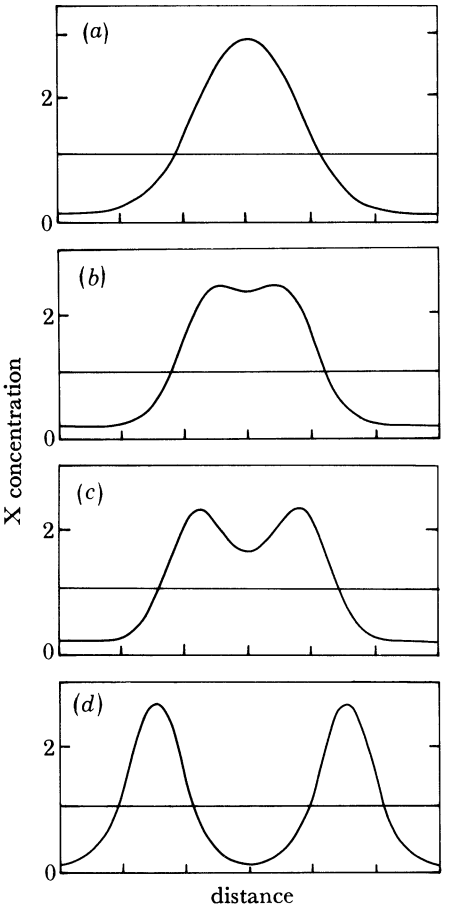

FIGURE 2. Branching of ternary pattern in a growing one-dimensional system.

With the ternary wave from figure 1*c* as a starting point, figure 2 shows the progressive bifurcation that occurs with gradual doubling of the effective length of the system (from 0.9 λ_m to 1.8 λ_m). The central maximum is driven down to produce two lateral peaks which move apart until they are twice as far from one another as each is from the boundary. Further increase in system length results in a similar and simultaneous branching of both peaks to give four equally spaced peaks. Such behaviour is obtained for a variety of parameter choices within the regions of parameter space giving stable spatial pattern (regions (*c*) and (*d*) in Lacalli & Harrison (1979)), and the parameters for figure 1 are located well within this region (see §8).

PHILOSOPHICAL TRANSACTIONS OF THE ROYAL SOCIETY B BIOLOGICAL SCIENCES

In contrast, if parameters are chosen so that k_g at λ_m is reduced towards zero, a different response is obtained (figure 3) for a comparable change in system length. The concentration gradient in X is itself much shallower, and new concentration maxima are generated at the boundary rather than the centre.

The above examples assume a uniform system in which parameter values are everywhere the same. It is not necessary that this be so. Rate constants may contain concealed concentration dependence (e.g. on catalyst concentration) and could therefore vary across the system. Gradients in viscosity across the system would have a similar effect on diffusivities. This means

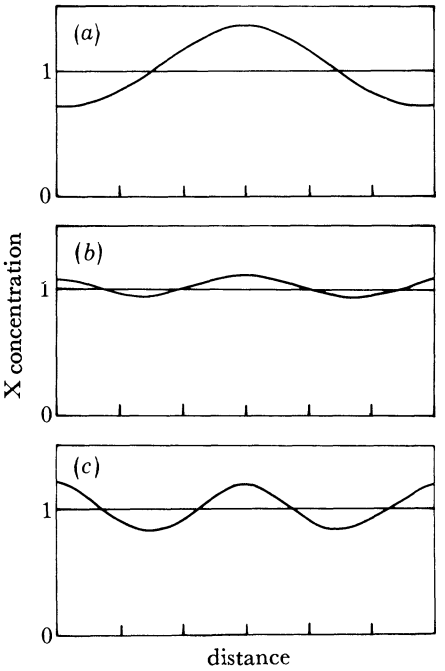

FIGURE 3. Branching of ternary pattern in a growing one-dimensional system with marginal pattern growth rate (k_g at λ_m is about $\frac{1}{25}$ that in figure 2).

that λ_m or k_g may vary over the system and that boundaries in parameter space separating regions of qualitatively quite different pattern behaviour may be crossed. This would considerably expand the possible range of patterns and pattern changes for even the simplest models. Given that gradients of various types can usually be demonstrated across the structures, cells or tissues participating in pattern-forming events in living organisms, it is appropriate to consider the effect on computations of gradients in parameter values. Figures 4 and 5 show two examples with a gradient introduced in the rate constant b and hence in the value of k_g at λ_m. In figure 4, b is twice as large at the boundary as at the centre; k_g at λ_m is then largest at the centre and gradually decreases, but is still positive, at the edges. The gradient is reversed in figure 5, with b twice as large at the centre as at the boundaries. Relative growth of the system to about three times its initial length (to 3.4 λ_m) produces three peaks in both examples, but by different means. In figure 4 there is an obvious struggle between the branching tendency at the centre (maximum k_g) and that near the boundary (minimum k_g), with the boundary finally winning. In figure 5, the usual splitting of the central peak occurs, but a third peak is then generated at the centre of the system (minimum k_g).

The author has not studied the effects of gradients in parameter values on pattern in great detail. The two examples in figures 4 and 5 are included primarily as a means of introducing the following two general points regarding such gradients.

(1) Parameter gradients offer an alternative to explicit boundary conditions. Reaction–diffusion models usually invoke either zero-flux (antinodal) or fixed-concentration (nodal) boundary conditions, or avoid the question by having an unbounded system (e.g. the surface

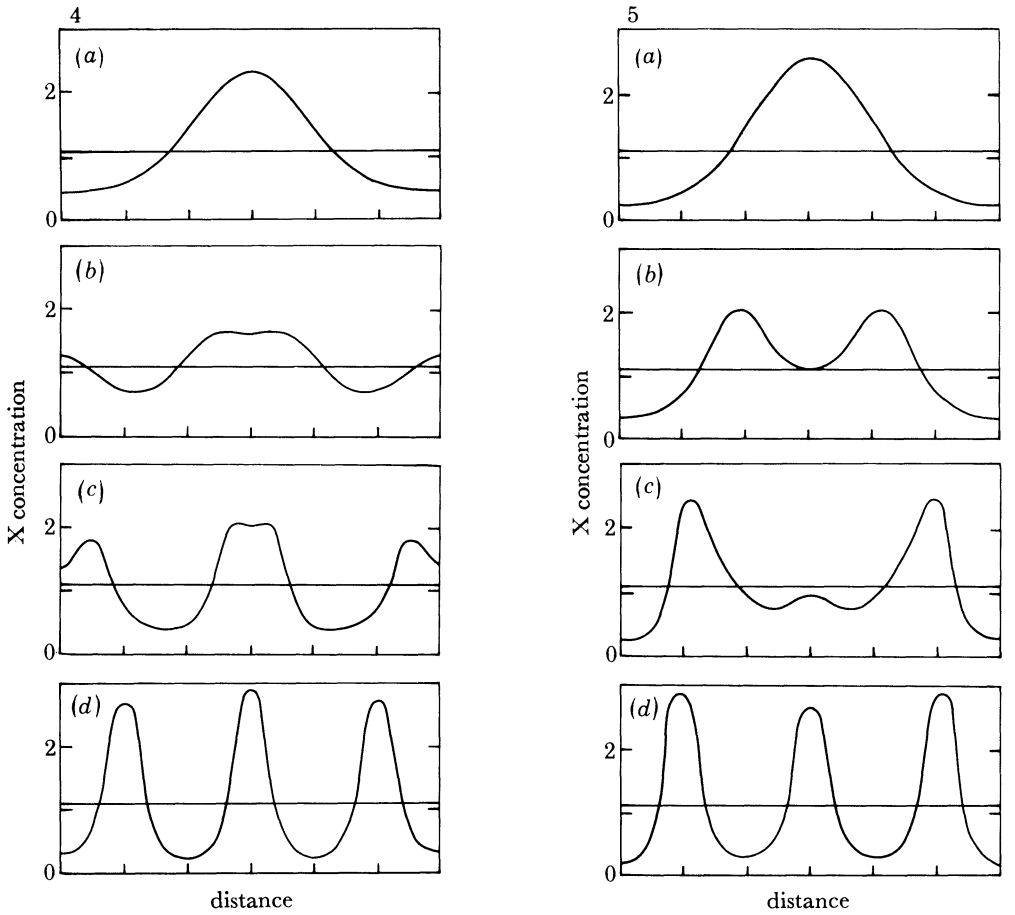

FIGURE 4. Branching of ternary pattern in a growing one-dimensional system with gradient in b (maximum b at edges).

FIGURE 5. Branching of ternary pattern in a growing one-dimensional system with gradient in b (maximum b at centre).

of a sphere) which translates into a periodic boundary condition in computations. It is not always clear how these different conditions are to be interpreted with regard to specific biological examples. The periodic boundary condition can be quite straightforward. A spherical surface, for example, would be appropriate for patterns generated on the surface of a spherical cell. The zero-flux condition makes sense for a chemical or biological system with discrete edges or boundaries. Interpreting the fixed-concentration condition depends to a much greater extent on the nature of the particular model being considered. In living organisms, boundaries do not always clearly separate the parts of a tissue or cell involved in pattern formation from those that are not. The use of parameter gradients may be the most appropriate means of dealing with such situations. Parameter values capable of supporting a pattern in one part of the

PHILOSOPHICAL TRANSACTIONS OF THE ROYAL SOCIETY B BIOLOGICAL SCIENCES

system would gradually reduce to values incapable of generating pattern in surrounding parts of the system. This is essentially what has been done in the computation shown in figure 15, in which a gradient similar to that in figure 4 is extended so that k_g is negative at the boundary. This allows pattern changes not permitted by the more conventional zero-flux and fixed-concentration boundary conditions.

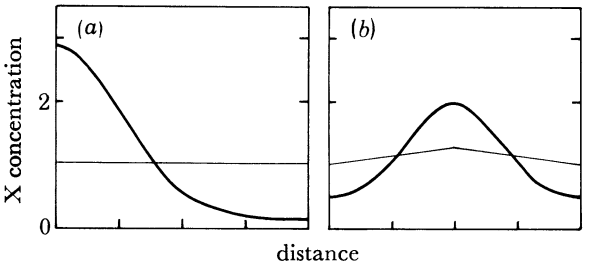

FIGURE 6. Patterns generated from steady state by random disturbances in a system with length in the binary region. (*a*) No parameter gradient. (*b*) Gradient in a (maximum a at centre).

(2) Parameter gradients may influence the generation of an initial waveform from random fluctuations. The same initial waveform, a well established ternary wave with central maximum, is used for both figures 4 and 5 despite the parameter gradient being reversed between the two. Random disturbances to the steady state will not generate this same waveform in both cases. In computations like that shown in figure 1 *a–c*, it is the gradient in figure 5 that produces a ternary wave with central maximum, while the figure 4 gradient gives a reverse ternary pattern with central minimum. This does not necessarily mean that the pattern change shown in figure 4 would be impossible in a biological system. Gradients may be supposed to come and go in a developing organism, so that an initial pattern might well develop under the influence of one gradient or set of gradients while growth and pattern change might not occur until a second set of gradients had been established.

Where several patterns are competing with one another, a further effect of parameter gradients will be to suppress some of these while favouring others. Gradients symmetrical about the centre of a system, as in figures 4 and 5, will suppress patterns that do not share this same symmetry. Ternary pattern can then develop even if the system is of a length such that k_g for binary pattern exceeds that for ternary. An example is shown in figure 6. The two patterns develop from random disturbances as in figure 1. For the length of the system ($l = 0.6\,\lambda_m$), k_g for binary pattern (from figure 11) is 1.8 times that for ternary. With no gradient, a binary pattern develops (figure 6*a*). With a modest gradient in a (a is increased by 16% at the centre) so that k_g is largest at the centre, binary pattern is suppressed in favour of ternary (figure 6*b*).

3.2. *Pattern arrays in two dimensions*

It is not immediately obvious what the two-dimensional equivalent of one-dimensional periodicity will be. Even if the resulting pattern is completely regular, either a square array or hexagonal array might be produced.

For Tyson's Brusselator, computations generate hexagonal arrays which develop by means of branching and movement of the morphogen peaks. Figure 7 shows the development of one such pattern. The computation is carried out on a square with edges approximately $3\lambda_m$ in length. Periodic boundary conditions are used so that the square (in dotted lines) is surrounded

on all sides by replicates of itself, portions of which are included in the figure to show the relative positions of the points more clearly. Initial conditions are steady-state values for X and Y, with random disturbances introduced throughout the computation. By 2000 iterations, nine peaks of comparable height emerge, giving a pattern with $R_2 = 1.846$. A period of peak branching and movement follows during which the pattern becomes progressively more regular. By 12000 iterations, 12 peaks are present and $R_2 = 2.00$. Spacing between peaks at this stage is roughly $0.85\ \lambda_m$. There is no reason to suppose that, if the introduction of random disturbances were

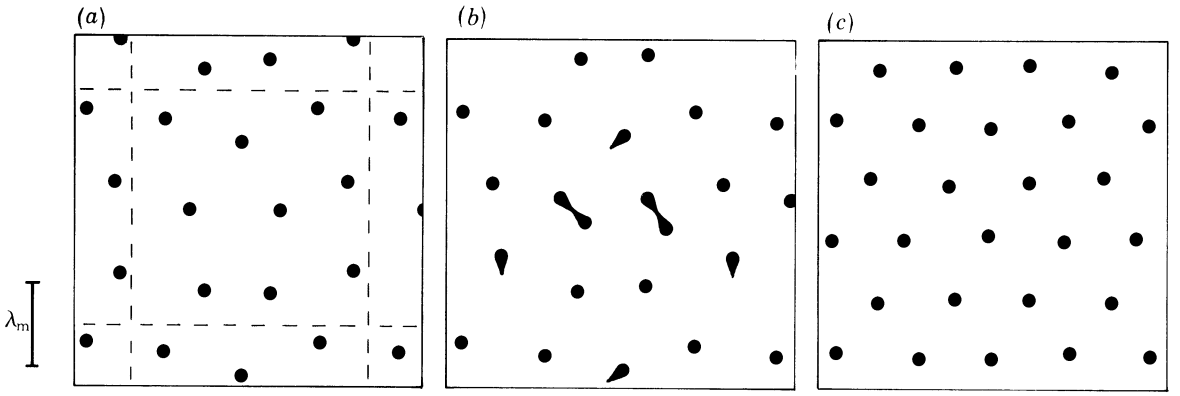

FIGURE 7. Stages in the generation of hexagonal pattern in two dimensions from steady state by random disturbances at (*a*) 2000, (*b*) 4000 and (*c*) 12000 iterations. Moving peaks are shown with their shoulders in (*b*).

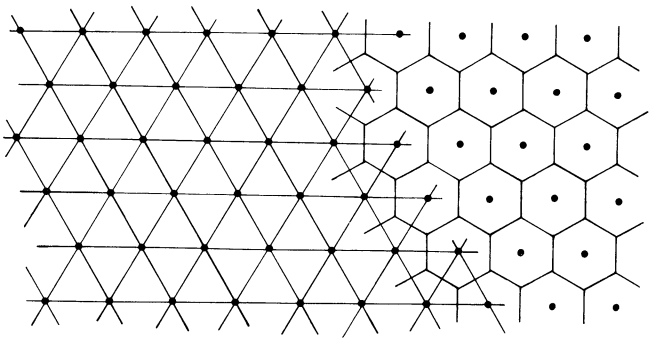

FIGURE 8. Six- and three-connected plane nets derived from a hexagonal array of points.

stopped, and given sufficient time, the pattern would not develop arbitrarily close to a perfect hexagonal array. Five additional computations like that in figure 7 were done with different ratios of λ_m to edge length of the square. All that were followed long enough showed the development of hexagonal pattern. The regularity of the outcome in these computations does not, therefore, appear to be dependent on a fortuitous choice of λ_m relative to system size. Measurements on the initial pattern of peaks for the four computations (including figure 7*a*) with clearly defined peaks gave a value for R_2 of 1.84 ± 0.03. In the two remaining cases the shoulders and varying heights of the peaks prevented determination of a meaningful value for R_2.

The nearness of figure 7*c* to a hexagonal array is evident by inspection. Each pattern point has six immediate neighbours roughly equidistant from one another. This represents a substantial improvement over figure 7*a*, for which, despite a relatively high R_2, choice of neigh-

PHILOSOPHICAL TRANSACTIONS OF THE ROYAL SOCIETY B BIOLOGICAL SCIENCES

bouring points and their number (five, six or seven) is much less obvious. With X maxima taken to be points of an array, the X minima can be approximated as a continuous plane net defining a domain around each point. For the hexagonal array, the corresponding plane net is a three-connected net of regular hexagons with a pattern point at the centre of each. This can be constructed as follows. Neighbouring array points are connected to give a regular six-connected net (figure 8, left side). Connection of the centres of adjacent triangles then gives the three-

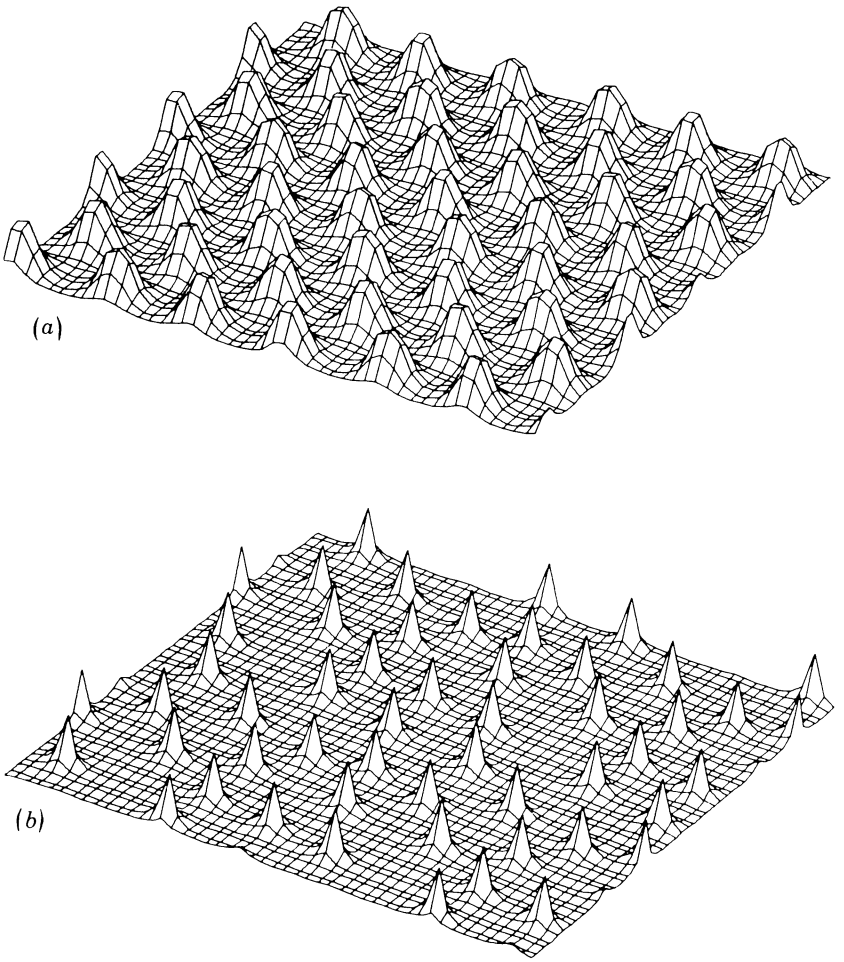

FIGURE 9. Patterns in a two-dimensional system, concentration along the vertical axis, for (*a*) Tyson's Brusselator, corresponding to the pattern in figure 7*c*, and (*b*) the Gierer & Meinhardt model. Calculated values for λ_m in (*a*) and (*b*) are 8.4 and 6.9 spatial units respectively.

connected net of hexagons (figure 8, right-hand side). As expected, the three-connected net corresponding with figure 7*c* is very close to being regular while an analogous construction with figure 7*a* gives a net with some five- and seven-sided polygons, depending on choice of neighbouring points. For some biological patterns, particularly if too few pattern points are visible for an order parameter like R_2 to be accurately calculated, nets of this type are a useful means of dealing with pattern order (see, for example, §4.1).

It is easily shown that the generation of hexagonal arrays is not a general property of all reaction–diffusion mechanisms. The model of Gierer & Meinhardt (1972), for example, generates patterns in two dimensions that are much less regular, and the morphogen peaks, once

formed, do not move. Figure 9*a* shows, in a three-dimensional plot, the concentration profile for X corresponding with figure 7*c*. This can be compared with the pattern generated by the Gierer & Meinhardt model, shown in figure 9*b* for their morphogen *a*. As in the previous two-dimensional examples, the computation was begun with steady state concentrations of both morphogens and pattern emerged from the continuous introduction of randomly placed fluctuations in concentration. For the pattern shown, $R_2 = 1.73$. The pattern is completely stable, and does not change with further computation.

3.3. *Branching on a circular disc*

This analysis of pattern change for a bounded two-dimensional system is done on a circular disc because the desmid septum, on which many characteristic desmid patterns develop, is initially circular. A hemispherical surface would better represent the shape of the septum at later stages (§4.2) and the hemispherical tips of growing semicell lobes, but the circular disc is applicable to these at least as a first approximation. Harrison *et al.* (1981), using a hemispherical system and Prigogine's Brusselator, obtain pattern changes very similar to those discussed here for the disc.

The spatial part of solutions for a circular disc to the linearized version of equations (1), expressed in polar coordinates (r, θ), are of the form

$$J_n(k_{nj}r)\cos n\theta,$$

where J_n is the nth Bessel function. Zeros in the derivatives of $J_n(\alpha)$ occur at particular values of the argument $\alpha = \alpha_{nj}$. For a disc of radius r_0 and zero-flux boundary conditions, the appropriate spatial mode, abbreviated J_{nj}, is obtained when the jth zero of the derivative of J_n occurs at the boundary. This fixes the value of k_{nj} associated with the mode J_{nj} for r_0 as

$$k_{nj} = \alpha_{nj}/r_0.$$

Figure 10 shows a selection of spatial modes that are relevant to interpreting the behaviour of Tyson's model on a disc. The subscript n corresponds with the number of radial nodes in the pattern, and j corresponds with the number of circular nodes. Spatial modes not encountered in any form in the computations have been left out. These include, for example, the $n = 1$ modes, having a single radial node and therefore less than twofold symmetry.

In discussing the development of patterns on a circle it is useful to have an equivalent, for the circle, of λ_m to serve as a measure of pattern size. The logical choice is that of the radius (r_m) at which growth of the J_{01} pattern is maximal, since this mode is roughly equivalent to a one-dimensional ternary wave rotated about its midpoint. Changes in system size are therefore given in terms of r_m, which is calculated as follows:

$$r_m = \alpha_{01}\lambda_m/2\pi \approx 0.61\lambda_m.$$

The calculation of growth rates for the various spatial modes follows that given by Lacalli & Harrison (1979) for one dimension, but with k_{nj} replacing ω ($=2\pi/\lambda$). Figure 11 shows plots of growth rate against radius for the patterns shown in figure 10, with a typical choice of parameters and with radius expressed in terms of r_m. Two one-dimensional patterns are included for a system of length l, also expressed in terms of r_m.

In the one-dimensional computations (§3.1), the starting point was a ternary pattern generated from random disturbances. The starting point for the computations in this section

is a single central morphogen peak, a nonlinear development of the J_{01} mode, with radius near r_m and zero-flux boundary conditions. This pattern is not easily obtainable from random disturbances. Instead, with zero-flux boundary conditions, patterns develop that correspond with modes of the $j = 0$ series of J_{nj} with concentration waves developed around the boundary and decaying to steady state values near the centre so as to give a kind of fluted disc appearance. The failure of the central peak to develop is not a particular problem in the present context since, in the biological examples to be discussed, the J_{01} pattern is not required to arise directly from the steady state. Altered boundary conditions or introduced gradients could, however, be used to encourage the development of the J_{01} pattern from disturbances to the steady state.

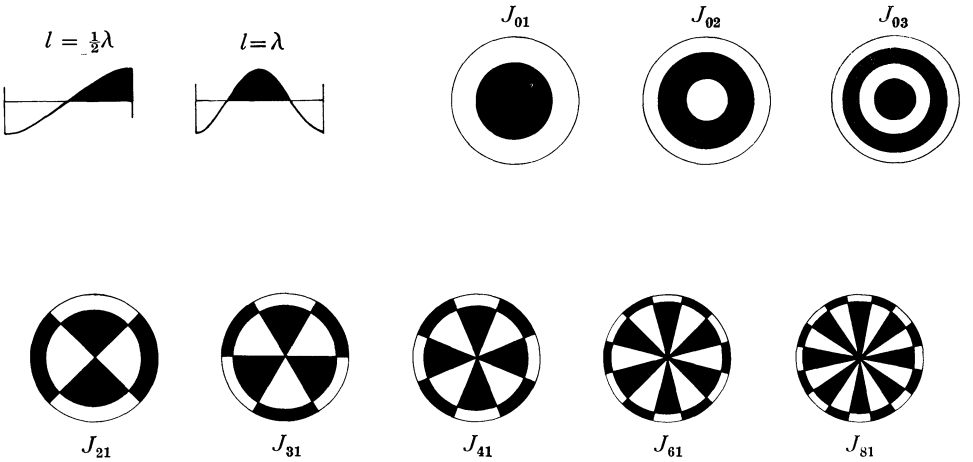

FIGURE 10. Selected pattern modes in one dimension and for the circular disc.

In a number of computations on discs and hemispherical surfaces by the implicit Crank–Nicolson method (Crank 1975), L. G. Harrison & G. D. Zeiss (personal communication and Harrison *et al.* 1981) have found the pattern changes accompanying increase in system size to be entirely dominated by radially symmetric pattern modes. Thus, on the disc, the initial peak (J_{01}) first flattens, then collapses in the centre to give a ring (J_{02}), which expands until, in some computations, a central peak reappears (J_{03}). The results of finite difference computations (figures 12, 13) show a similar pattern sequence in early growth stages, but various types of circumferential branching occur as growth proceeds to give patterns resembling members of the $j = 1$ series of pattern modes. There is a considerable overlap of growth rate curves for the various $j = 1$ modes (figure 11), and a number of these have quite similar growth rates in the size range under consideration. Only selected modes appear, however, for the most part being those whose symmetry corresponds with the biases and artefacts inherent in the computations. In figure 13, a square grid with the corners removed is used to approximate circular shape. The boundary, in fact, then has fourfold symmetry, and the patterns that develop also have fourfold symmetry. In figure 12, a 24-fold symmetry is imposed on the computation by the choice of the angular increment, and the symmetry of the resulting pattern is related as a simple multiple. This sensitivity to global features of the system such as symmetry, boundaries and boundary conditions is a well known characteristic of nonlinear reaction–diffusion equations (see, for example, Bunow *et al.* 1980) and of nonlinear equations in general.

The computation shown in figure 12 was done in polar coordinates, the angular component

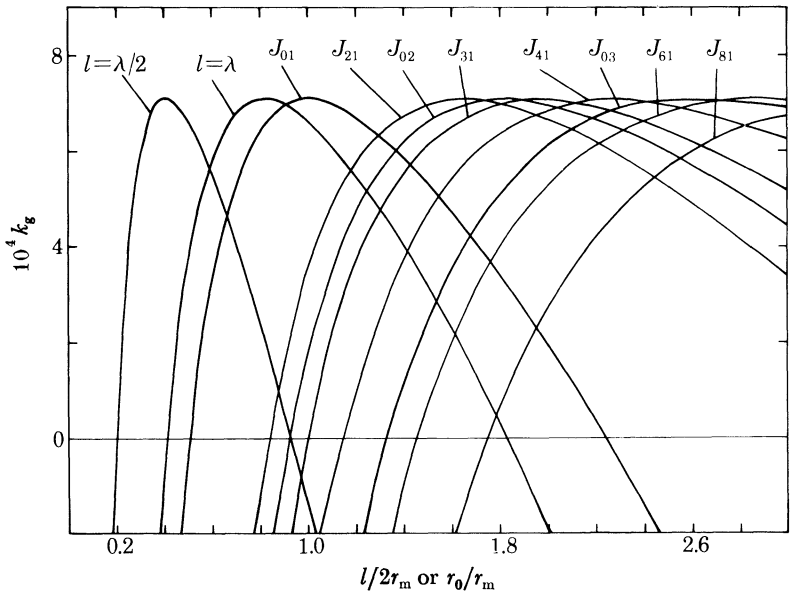

FIGURE 11. Growth rate (k_g) against system size for the pattern modes shown in figure 10. The graph shows, for a given system size, the relative magnitude of k_g for the various pattern modes that can develop (i.e. $k_g > 0$) at that size. Size, as length (l) for one-dimensional pattern or radius (r_0) for the disc, is scaled to r_m.

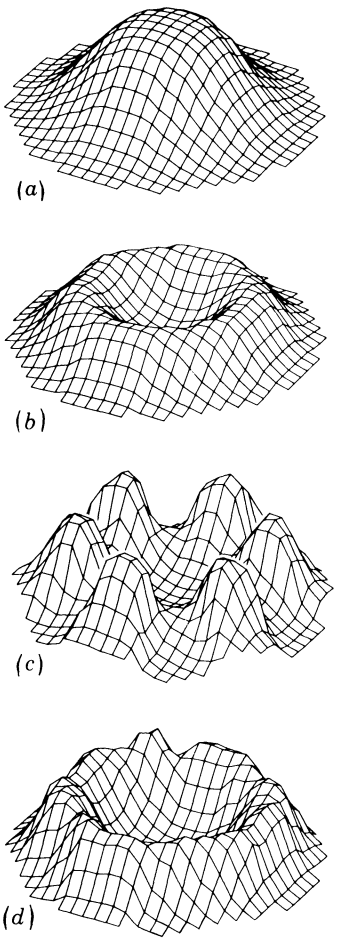

FIGURE 12. Pattern change on a growing disc, calculation in polar coordinates.

PHILOSOPHICAL TRANSACTIONS OF THE ROYAL SOCIETY B BIOLOGICAL SCIENCES

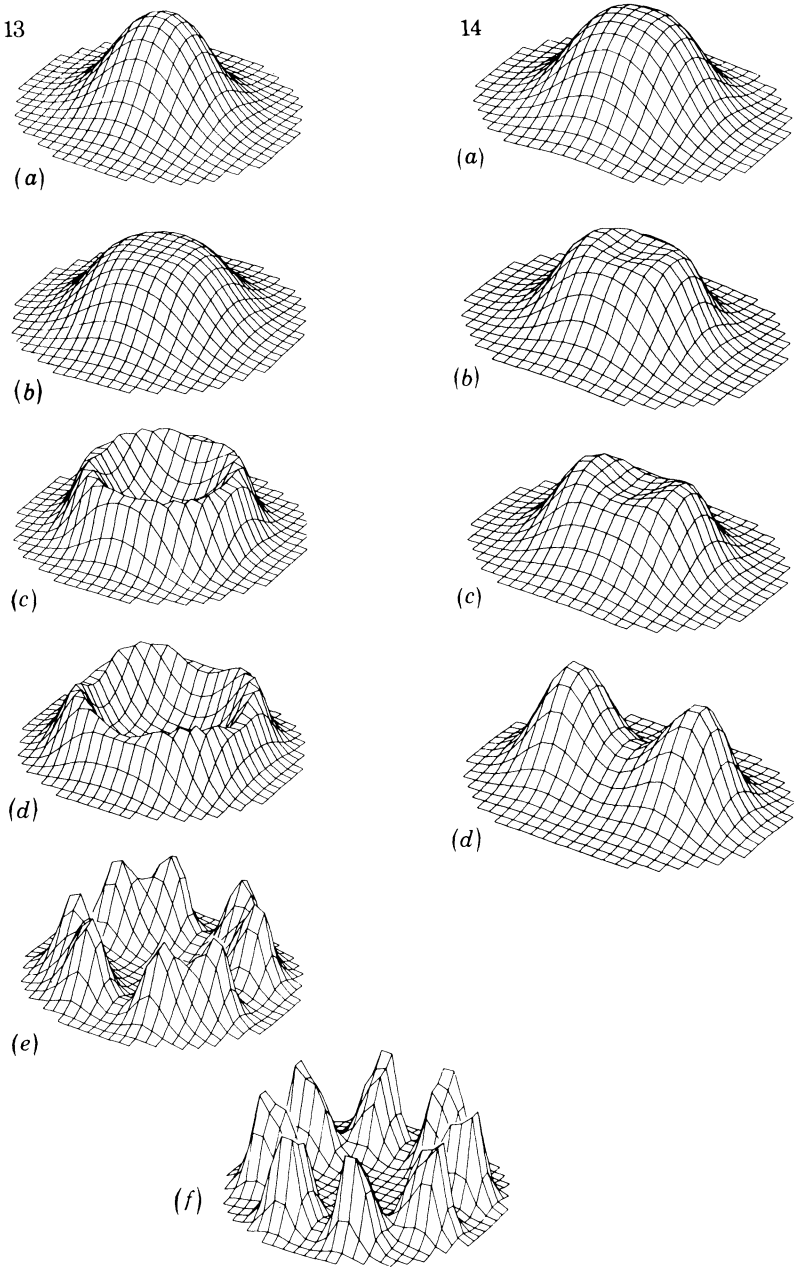

FIGURE 13. Pattern change on a growing disc, calculation in Cartesian coordinates.
FIGURE 14. Pattern change on a growing disc with twofold symmetry, approximating an oval.

being divided in relatively coarse increments of $\pi/12$ for reasons of cost, and plotted on a Cartesian grid. System size is 0.96, 1.36, 1.52 and $2.15r_m$ respectively in figure 12*a–d*. If growth is slow and continuous, the entire sequence is observed, each pattern being characteristic of a particular size range and stable to introduction of random disturbances at that size. J_{61} is the only pattern mode of the $j = 1$ series to appear, despite the fact that J_{31}, J_{41} and J_{81} have positive growth rates through much of the size range, and symmetry compatible with the computational grid. J_{61} develops very slowly, however, and is only transient. Rapid growth to $2.15r_m$ would prevent its appearance entirely.

Figure 13 shows the pattern change in a computation in Cartesian coordinates for growth from $0.81r_m$ (figure 13*a*) to 0.95, 1.15, 1.40, 1.82 and $2.15r_m$ respectively in figure 13*b–f*. The initial conversion of J_{01} to J_{02} is followed by a sequence of patterns combining elements of J_{02}, J_{41} and J_{81} to give first four and then eight peaks. Patterns that are not compatible with the fourfold symmetry of the system, including J_{21}, are completely suppressed. A situation in which J_{21} does dominate over J_{02} is shown in figure 14. Here the system is given a marked twofold symmetry by trimming off two sides so that an approximately oval shape is obtained, with a length to width ratio of 1.2. Growth is from $0.81r_m$ for half the long axis in figure 14*a* to $1.15r_m$ in figure 14*b–d*, which shows the progressive development at this size of a dichotomous branch oriented along the long axis.

From these and a number of additional computations on a disc, including some with introduced gradients, the following general conclusions emerged. Pattern modes corresponding to small n values ($n = 2$ or 3) dominate over J_{02} only when strongly favoured by system symmetry, as in figure 14. Within an intermediate range ($n = 6$–8) whorls of distinct peaks form much more readily, but patterns corresponding to large n values ($n > 12$) cannot be obtained in the same fashion. Before the J_{02} pattern can expand sufficiently relative to r_m to give large numbers of peaks, some radial pattern change will occur. This usually involves the appearance of a new peak at the centre of the disc or an additional ring of peaks around the boundary, or radial splitting of the existing structure. It is therefore not possible to generate arbitrarily large numbers of peaks in a single whorl by means of Tyson's model alone.

Despite boundary effects, a dichotomous branch can be generated on a circular disc if the boundary conditions are appropriately adjusted. This is shown in figure 15, where, as in the one-dimensional case illustrated in figure 4, a radial gradient in b is introduced so as to leave a rim around the central peak where k_g at λ_m is negative. The actual boundary of the computation is then well separated from the region in which pattern develops, and this appears to damp out the effect of the boundary. The initial pattern (figure 15*a*) occupies a disc with radius $2.1r_m$. Modest growth, to 1.56 times this initial size allows a dichotomous branch to form at the centre. A second pair of peaks, oriented at right angles to the first, develops more slowly at approximately the point on the radial gradient at which k_g goes to zero. The unusual boundary conditions prevent ready comparison of system size between figure 15 and the previous examples. If, however, the distance from the disc centre to the X minimum in figure 15*a* is taken as roughly representative of an effective r_m ($=r'_m$) for the computation, then growth is: to $1.27r'_m$ in figure 15*b*, then to $1.56r'_m$ in figure 15*c*, with progressive stages of pattern development at this size shown in figure 15*c–e*. At $1.56r_m$, growth rate for the dichotomous pattern, J_{21}, exceeds that of the other competing patterns (figure 11). Subsequent movement of the four peaks in figure 15*e*, inward for the outer pair and outward for the central pair, suggests that stability would be achieved only with all four equidistant from the centre. Pattern changed very slowly during the later stages of the computation; so it was not followed to a stable endpoint. Figure 15 fails to produce the desired pattern, that is, a stable dichotomous branch. The twofold symmetry of the early computational stages could, however, be saved and, in fact, amplified by making some additional assumptions about what happens to the system between the time of the first appearance of the branch and the final fourfold, or nearly fourfold, symmetry. It could be supposed, for example, that the morphogen was involved in the control of system growth. If high morphogen concentration resulted in localized expansion in area, the effect of a pattern like that in figure 15*c* in terms of growth in the system would be twice as great along the axis of the branch as at right angles to the axis. Such asymmetric growth could very readily establish

PHILOSOPHICAL TRANSACTIONS OF THE ROYAL SOCIETY B BIOLOGICAL SCIENCES

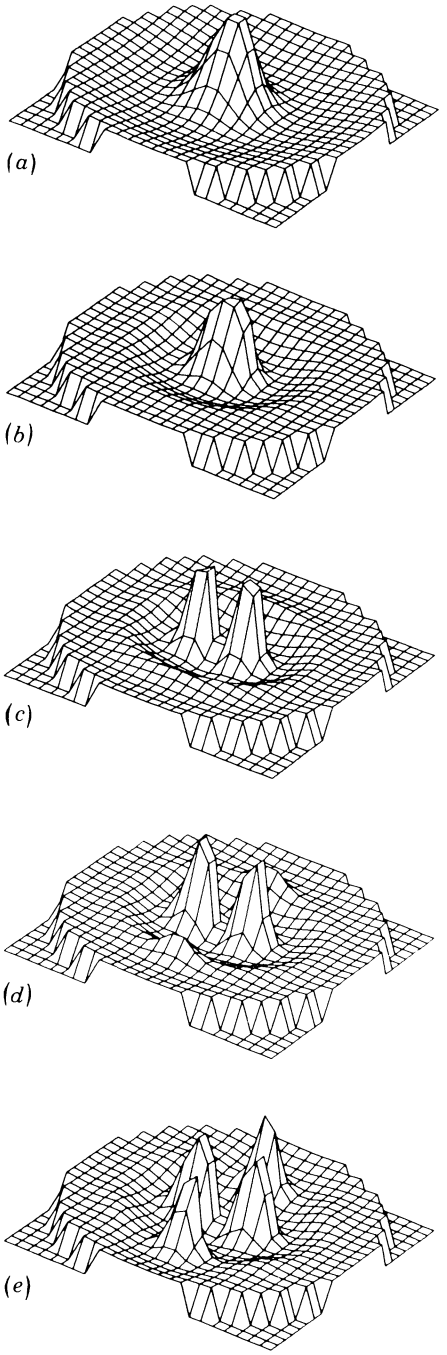

FIGURE 15. Pattern change on a growing disc with gradient in b (maximum b at the boundary).

a twofold symmetry in system shape sufficient to completely suppress the more slowly developing fourfold pattern.

In summary, the general properties of Tyson's Brusselator include the generation of harmonic and periodic patterns, the latter giving hexagonal arrays in two dimensions, and of rings and whorls of peaks on a growing circular disc. The final outcome of the latter pattern change, whether ring or whorl of peaks, is strongly dependent on boundary effects and biases in the

PHILOSOPHICAL TRANSACTIONS OF THE ROYAL SOCIETY B BIOLOGICAL SCIENCES

computation. This does not invalidate the computational work discussed in this section since various biases, operating through symmetry features, gradients or structural anisotropies, may well be involved in the development of many biological patterns.

4. Desmid patterns

4.1. *Zygospores*

Desmids have both a vegetative phase in which clones of cells are produced by repeated mitosis, and a sexual phase in which fusion of two vegetative protoplasts results in formation of a thick-walled zygospore (figure 16). Desmid zygospores are spherical or nearly so in most

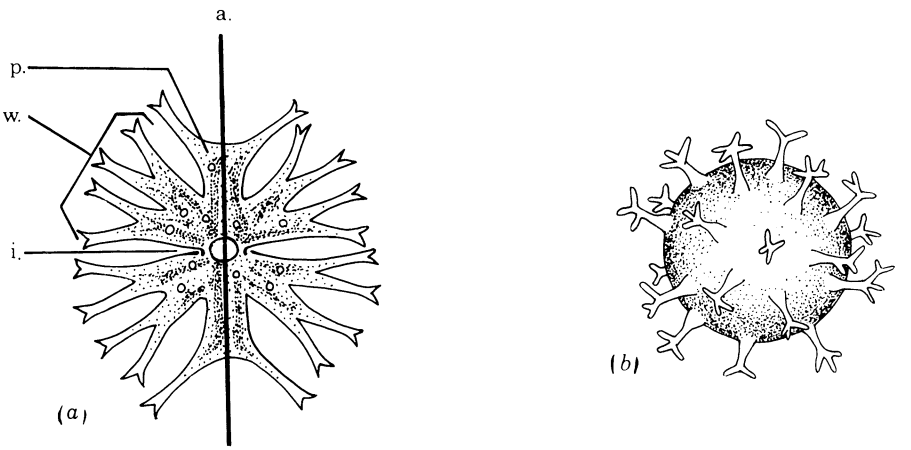

Figure 16. *Micrasterias*. (*a*) Vegetative cell of *M. radiata* showing polar lobe (p.), one lateral wing (w.), isthmus (i.) and polar axis (a.). (*b*) Zygospore of *M. denticulata*. From West & West (1905, vol. 2). (Magn. × 200.)

species and are usually ornamented with spines. These develop as localized outgrowths from the initial wall produced by the fused protoplasts. The spines appear to elongate by means of tip growth (Kies 1970) and, in many species, develop terminal branches (see, for example, figure 16*b*). A thick inner wall is then deposited with use of the initial wall as a template, and this becomes the wall of the mature zygospore.

Published drawings of a number of desmid species show the zygospores' ornamentation, but special attention has seldom been paid to the exact arrangement and spacing of the spines, which, in the present context, is their most significant feature. Because of the zygospores' curvature and opacity, light micrographs fail to show spine patterns clearly. Scanning electron micrographs, which give a three-dimensional view of the surface, are far more revealing. Although relatively few such micrographs have yet been published, those that have establish without question the basically hexagonal arrangement of the spines to give pattern arrays with degree of order very similar to that seen in the *Tagetes* pattern discussed in §2. The majority of scanning micrographs show only the mature zygospores, whereas what is really needed is a complete survey of pattern development from the first appearance of spine initials, as has been done for *Tagetes*. Because desmid zygospores do not expand or change shape during spine development, however, the final spine pattern can be taken as a good approximation of the pattern of spine initiation.

A *Cosmarium* zygospore is shown in figure 17. Because of surface curvature and the coat of

PHILOSOPHICAL TRANSACTIONS OF THE ROYAL SOCIETY B BIOLOGICAL SCIENCES

mucus obscuring many of the spines, spacing cannot be measured between enough spines for a meaningful analysis of the pattern as a whole. The tendency to local hexagonal order for the few spines visible can, however, be made clear by constructing the corresponding plane nets described in §3.2. These are shown in figure 18. The local ordering is, by eye, close enough to the hexagonal pattern generated by Tyson's Brusselator (figure 7*c*) that values of R_2 close to 2 for the pattern would not be surprising.

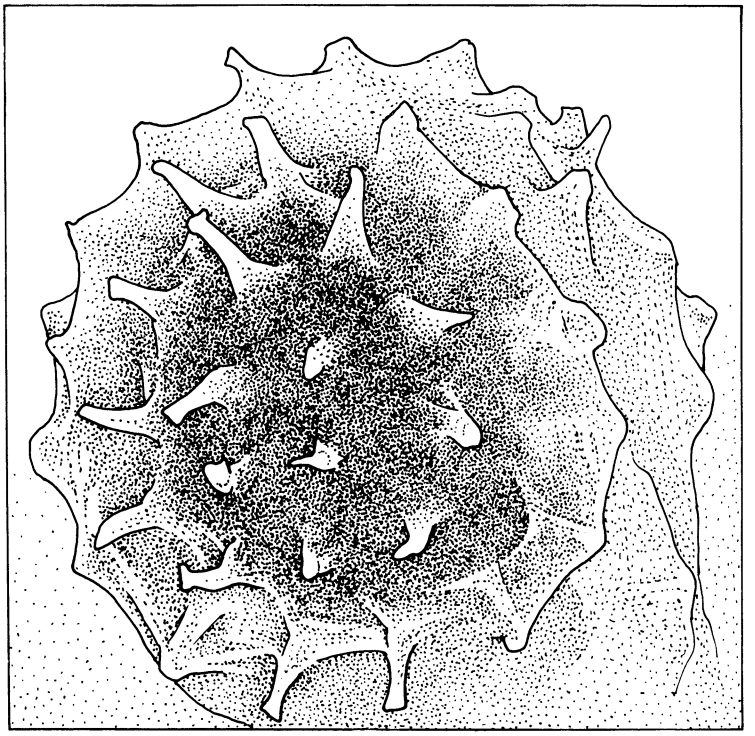

FIGURE 17. Zygospore of *Cosmarium botrytis*. From a scanning micrograph, fig. 17 of Pickett-Heaps (1974). (Magn. × 1600.)

Arrays of hexagons as in figure 18*b* can be extended indefinitely to fill a plane, but will not form a closed surface. Introducing polygons with fewer sides into the array will accomplish this where, following Euler (Thompson 1942), if only pentagons are used, exactly 12 would be required. A large number of polyhedral surfaces are then possible having 12 pentagonal faces and various numbers of hexagonal ones (see Crowther *et al.* 1976, for examples). *Cosmarium* zygospores oblige by having some pentagons in their pattern array: spines with five regularly spaced neighbours are visible in some of the micrographs (see, for example: Pickett-Heaps 1975, fig. 6.165; Berliner & Guth 1979, figs 4, 6). For zygospores that are smaller relative to interspine distance than *Cosmarium*, the proportion of spines with five neighbours should increase relative to those with six. In fact, pentagonal arrangements are more numerous in published pictures of *Staurastrum furcigerum* zygospores (figure 19), in which the ratio of interspine spacing to spore diameter is 1:3, compared with a ratio of about 1:7 for *Cosmarium botrytis*.

The author has not followed the behaviour of Tyson's Brusselator on a spherical surface in computations; so it is not clear what the analogue of the hexagonal pattern developed by the model on a plane would be on a curved surface. For a sphere chosen of appropriate size to

accommodate exactly 12 pattern points, placing these at the vertices of an icosahedron is the most likely solution as it gives the most regular possible arrangement, each point having five equivalent neighbours. It remains to be seen how pattern points in excess of 12 would be incorporated into this initially pentagonal array, but a mixture of pentagons and hexagons as seen in the zygospores themselves seems a reasonable possibility.

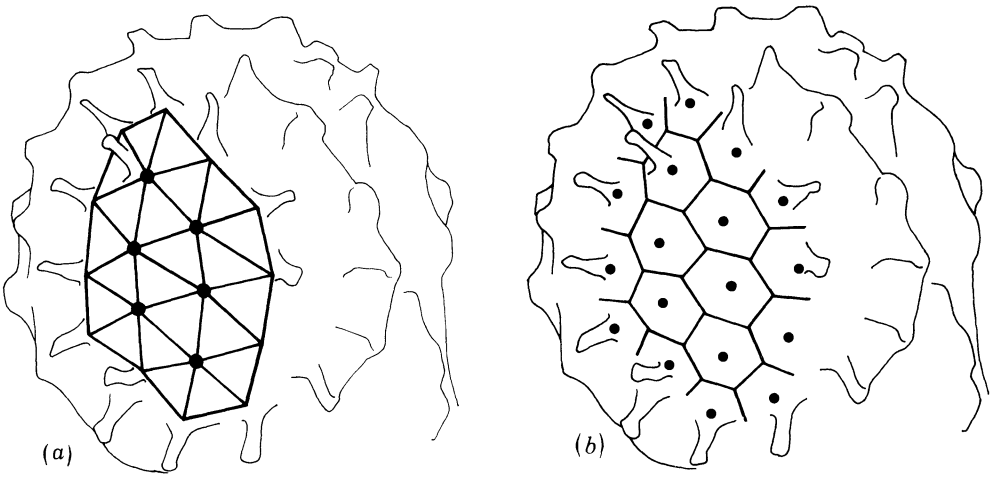

FIGURE 18. The arrangement of spines on the *Cosmarium* zygospore shown in figure 17 with the corresponding plane nets drawn in. (Magn. × 1030.)

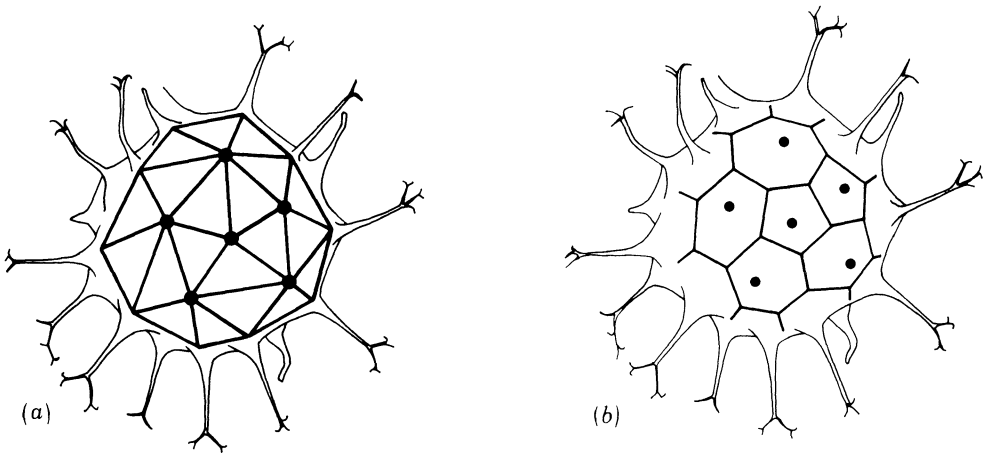

FIGURE 19. The arrangement of spines on a zygospore of *Staurastrum furcigerum* with the corresponding plane nets drawn in. From a scanning micrograph, fig. S8, appendix I, Pickett-Heaps (1975). (Magn. × 640.)

4.2. *Patterns in dividing cells*

In the placcoderm desmids, a typical vegetative cell consists of two halves, or semicells, joined by overlap at an isthmus which is usually narrower than the rest of the cell and so appears as a constriction (figure 16*a*). The principal axis of the cell, the polar axis, passes through the two semicells and the isthmus. In *Micrasterias*, as shown (figures 16*a*, 20*a*), each semicell has a central polar lobe and two oppositely placed lateral wings. Thus there is twofold rotational symmetry about the polar axis. Other desmid genera and certain abnormal forms of *Micrasterias* have other symmetries.

PHILOSOPHICAL TRANSACTIONS OF THE ROYAL SOCIETY B BIOLOGICAL SCIENCES

Like zygospores, vegetative cells may be ornamented with a variety of bumps and spines. The evidence suggests that similar mechanisms may be involved in the formation of these structures regardless of the life history stage at which they appear.

(1) Whether on zygospore or vegetative cell, the structures often have very similar morphology. For example, the slender branched lobes into which lateral wings of *M. radiata* are divided (figure 16*a*) closely resemble the spines of many *Micrasterias* zygospores. And, as a survey of West & West (1904–1923) readily shows, the desmid genera with the most highly ornamented vegetative cells (*Micrasterias*, *Staurastrum*, *Xanthidium*) tend also to have the most elaborate zygospore ornamentation.

(2) The cell walls involved in morphogenesis in both cases are very similar in appearance in electron micrographs (Kies 1970; Kiermayer 1970*a*). Both are of the primary wall type, that is, thin and composed of randomly oriented cellulose microfibrils. The primary wall is a temporary structure in both cases, the final wall being the result of secondary deposition for which the primary wall serves as a template.

(3) Morphogenesis is by means of tip growth in vegetative cells (Lacalli 1975*a*), and this is undoubtedly also the case in zygospores (Kies 1970).

Although the patterns of ornamentation seen on vegetative cells are far more varied and complex than the simple pattern arrays characteristic of zygospores, this paper proposes that patterning is governed by the same reaction–diffusion mechanism in both. No other satisfactory explanation has been proposed for pattern in either case. For example, despite an extensive search, no evidence for an underlying cytoplasmic order that might influence semicell shape has as yet been discovered (Selman 1966; Kiermayer 1970*b*). Kies (1970) found the distribution of some cytoplasmic organelles to parallel the morphogenetic pattern in zygospores, but has not shown this to be of causal significance.

The events involved in replication of species-specific semicell pattern following mitosis are shown in figure 20 for *Micrasterias*, the genus most extensively studied in this regard. A girdle of primary wall material is first deposited on the inside of the secondary wall at the isthmus (figure 20*b*). This thickens and widens so as to allow the semicells to detach and separate from one another. A septum is then established around the circumference of the girdle at its midpoint (figure 20*c*). Inward growth of the septum separates the cytoplasm of the two daughter cells by telophase, while progressive splitting of the septum results in two flattened hemispherical bulges at the stage shown in figure 20*d*. To this point the new primary wall is, as far as can be distinguished, entirely symmetric about the polar axis. Subsequent development (figure 20*e*) produces a twofold symmetry corresponding to that of the parent semicell. This is seen in the three-lobe stage as growth sites responsible for the two lateral wings and polar lobe are established. Repeated bifurcation of the lateral sites produces, in succession, five-, nine- and seventeen-lobe stages. The three-lobe stage is thus quite transient, but evidence for its existence as a distinct stage is available from u.v. irradiation studies (Waris & Kallio 1964; Hackstein-Anders 1975) and laser damage tracings (Lacalli 1975*a*).

A proposal as to how Tyson's Brusselator might produce the patterns in figure 20 is shown in figure 21. With appropriate assumptions, the pattern sequence in *Micrasterias* to the three-lobe stage can be accommodated. The initial extent of the girdle appears to be defined by the nature of the adjacent secondary wall (Lacalli 1973). Deposition is at first uniform, suggesting that any governing morphogen must be evenly distributed, that is, at uniform, steady state concentrations. If one assumes that some increase in girdle width can occur as a consequence, the critical

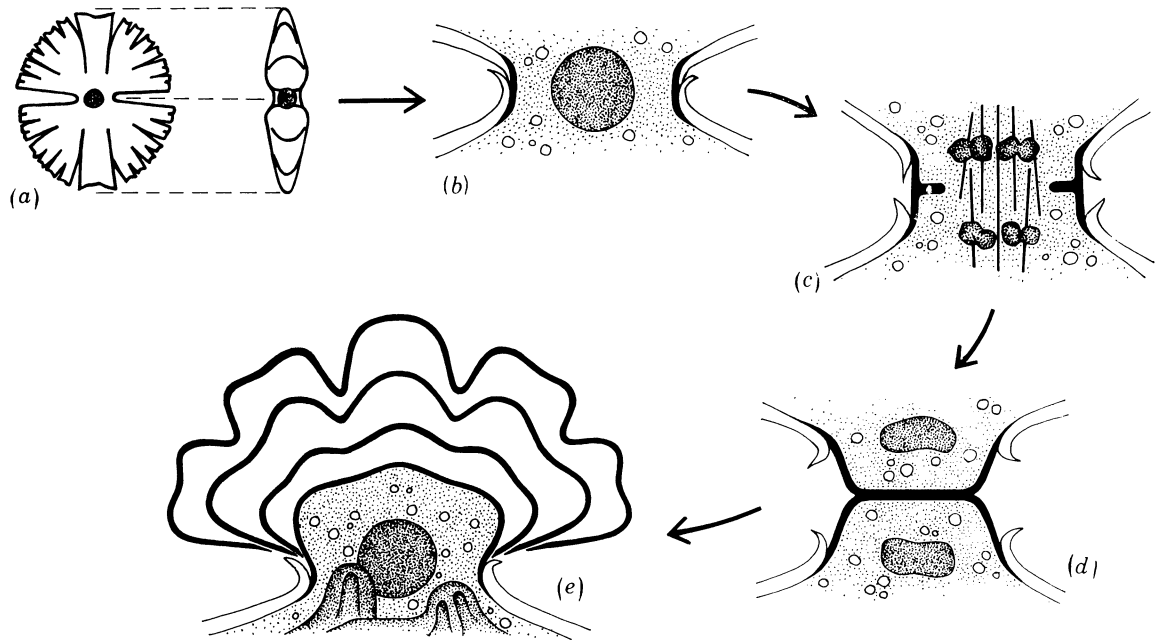

FIGURE 20. Mitosis, septum formation and morphogenesis in *Micrasterias*. After Lacalli (1973, 1975*a*).

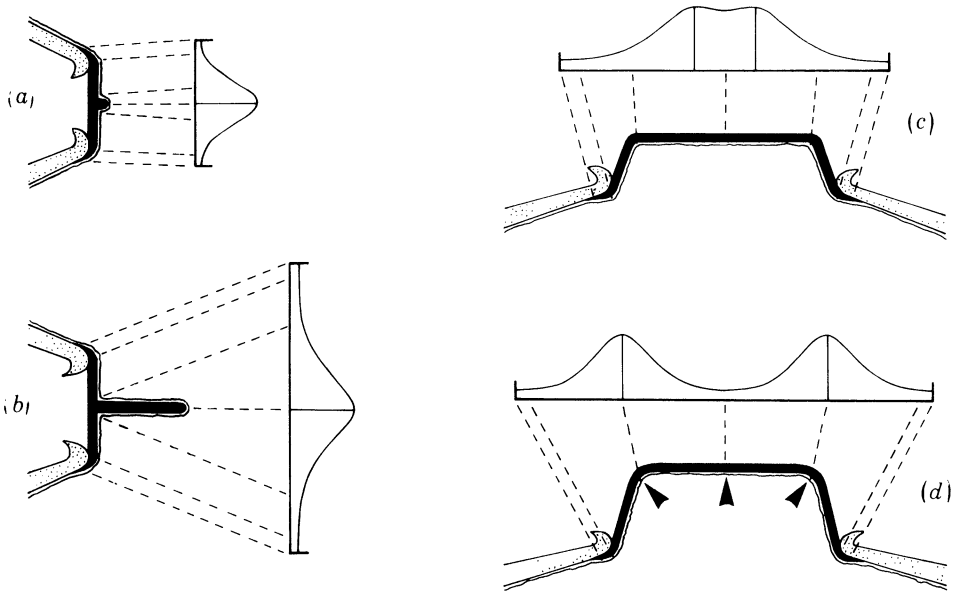

FIGURE 21. One-dimensional pattern modes matching the sites of wall deposition on girdle and septum as seen in section. For genera in which rings or rings of spines develop, the third dimension for (*a*)–(*d*) is simply a figure of rotation about the polar axis. For *Micrasterias*, (*c*) and (*d*) would be sections through a dichotomous branch which, in three dimensions, corresponds to a pattern change like that shown in figure 14. Initiation sites for the three semicell lobes (according to Lacalli 1975*a*) are indicated by arrows in (*d*).

PHILOSOPHICAL TRANSACTIONS OF THE ROYAL SOCIETY B BIOLOGICAL SCIENCES

size for ternary pattern across the width could be crossed. For ternary pattern with central maximum, if concentration maxima result in localized wall deposition, a septum-like ingrowth will be established at the midpoint (figure 21*a*). Ingrowth will continue (figure 21*b*) as long as the surface occupied by the morphogen wave, taken here as the inside surface of the wall or the membrane, remains within the size range for ternary pattern. When the annular septum has completed its separation of daughter cells, two separate morphogenetic systems are created, comprising the inside surfaces of the two hemispherical bulges (figure 21*c*). The waveform

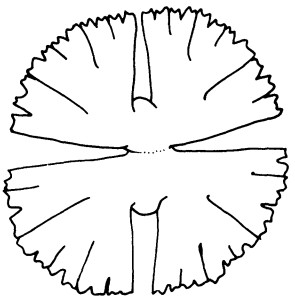

FIGURE 22. *Micrasterias denticulata*, cell from a mutant clone lacking the polar lobe. From unpublished micrographs supplied by D. H. Tippit & J. D. Pickett-Heaps. (Magn. × 270.)

inherited by each from the previous stages of septum growth has a central maximum, thus corresponding to the initial pattern used in circular disc calculations in §3.3. The appearance of growth sites in various patterns on the hemispherical bulge in different desmid genera following septum completion suggests that this event should correspond with branching of the governing morphogen wave (figure 21*d*). Examples can be cited giving growth patterns suggestive of a dichotomous branch (*Micrasterias*, disregarding the polar lobe), rings, or whorls of peaks (*Bambusina* and *Staurastrum*, see below). For these examples, beyond qualitative pattern similarities, the relative proportions of girdle, septum and branch points should be quantitatively comparable. The sequence proposed in figure 21 requires further discussion, however, before the qualitative predictions of the model are examined (§4.3).

(i) *The polar lobe*

The *Micrasterias* polar lobe is not accounted for in the above sequence since the central peak is lost when dichotomous branches form (e.g. figures 14, 15). In a previous analysis of *Micrasterias* morphogenesis (Harrison & Lacalli 1978), the polar lobe and wings were considered together as consequences of a linear wave pattern with three morphogen peaks. The three lobes were therefore taken to be identical, at least with regard to the means of their initiation. With Tyson's model, there are various ways to regenerate the central peak following branching (e.g. with parameter gradients), but the author has been unable to do this in conjunction with a dichotomous branch. The desired pattern, a single row of three peaks across one axis of a circular disc, appears to be incompatible with the symmetry of the disc.

There may, however, be no need to specify the polar lobes and lateral wings by a single mechanism. Lateral wings must be precisely positioned on an otherwise undistinguished expanse of septum wall. The polar lobe arises at the centre of the hemispherical bulge at a point already distinguished from surrounding wall by being the point of closure of the growing septum. The polar lobe is itself not an essential part of the pattern. Mutant strains have been

isolated that lack this lobe altogether, yet have normal wings (figure 22). And in double cells produced by failure of the septum to close, the wing lobes, which must then be specified on an annulus rather than a disc, are often normal while the polar lobe is missing. The polar lobe differs from the wings in several respects. Beyond the obvious differences in shape and degree of branching, there are differences in patterns of wall deposition and response to laser damage (Lacalli 1975*b*). It therefore may not be an essential test of a morphogenetic model that it account for the polar lobe.

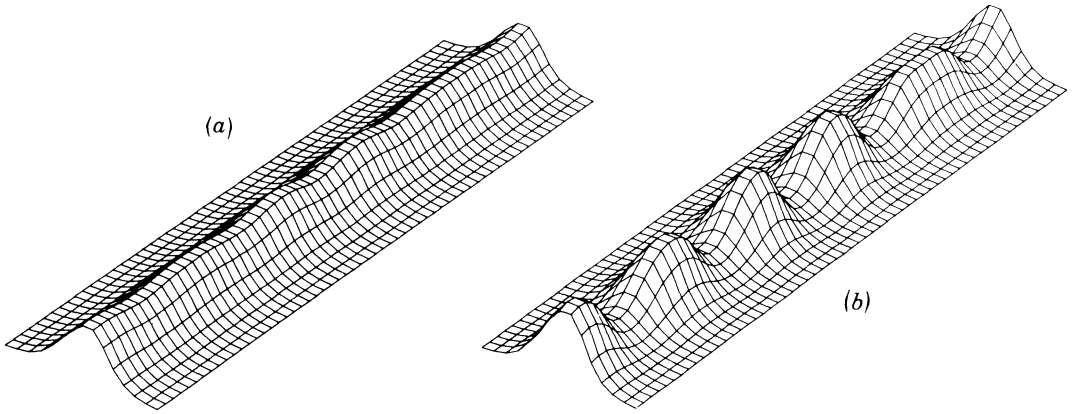

FIGURE 23. Pattern generated on a narrow band from steady state by random disturbances, gradient in a across the width, with maximum a along the midline. (*a*) An early computational stage. (*b*) The final pattern.

(ii) *Establishing the septum*

By means of Tyson's Brusselator, it is not a simple matter to establish the waveform that would be required to generate the septum. A ternary wave with central maximum is needed across the width of the girdle, and binary pattern must be suppressed. In addition, ternary pattern must be maintained uniformly along the whole circumference of the girdle even though this is substantially greater than girdle width. The first of these requirements is easily satisfied by introduction of a gradient with symmetry about the middle of the girdle. This both guarantees the central maximum and suppresses binary pattern (as in figure 6*b*). Such a gradient is by no means unreasonable in biological terms. The girdle has a corresponding symmetry in structure, being thinner at the edges than in the middle, and, because it lies exactly between the two semicells, the arrangement of cellular structure around it has this same symmetry. The author has not, however, been able to satisfy the second requirement, of preventing the appearance of peaks around the circumference. The problem is illustrated in figure 23. With a symmetrical parameter gradient across the width corresponding to that in figure 6*b*, the desired waveform appears initially from random disturbances as shown in figure 23*a*. This then develops, in all the computations tested, into a row of peaks (figure 23*b*). One way of resolving this problem within the context of reaction–diffusion theory is to assume the girdle to be anisotropic with regard to diffusion. To get the desired pattern, diffusion would have to be slower and λ_m consequently smaller across the width of the girdle than around its circumference. This is not the only situation in plants in which this type of anisotropy may be required for pattern to be explainable in reaction–diffusion terms. Regularly spaced ring-like thickenings are characteristic of xylem cells in many vascular plants (see, for example, Hepler & Fosket

PHILOSOPHICAL TRANSACTIONS OF THE ROYAL SOCIETY B BIOLOGICAL SCIENCES

1971). Here also the longitudinal spacing, between rings, is much less than the circumference of the cell, yet the rings appear to be deposited uniformly around this circumference.

Many elongate or cylindrical algal cells divide by forming septa midway along their length or at the midpoint of separate, internal wall structures as in the desmid girdle or the formation of H-shaped wall segments in *Microspora* (Pickett-Heaps 1973). Given the potential of ternary waves to specify the midpoint of structures on which they develop, reaction–diffusion mechanisms could be employed quite generally by cells as a means of positioning such septa. Classic experiments by van Wisselingh (1909) on *Spirogyra* are generally interpreted as providing

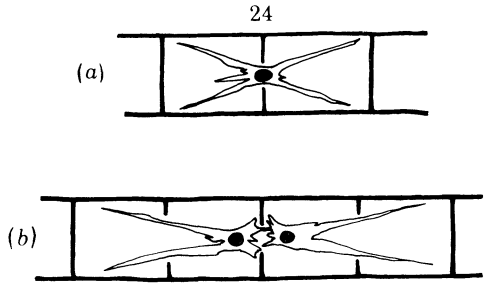

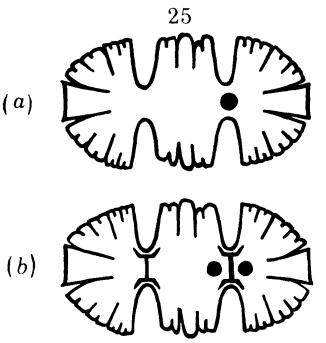

FIGURE 24. Formation of septa at an unusual position in *Spirogrya*; (*a*) and (*b*) from figures 13 and 20 respectively of van Wisselingh (1909).

FIGURE 25. Mitosis and septum formation in double cells of *Micrasterias*. After Waris & Kallio (1964).

evidence to the contrary. Van Wisselingh used centrifugation to displace cell nuclei along with much of the cells' cytoplasm, and observed that the site of septum formation was likewise displaced in many instances. He concluded that the position of the nucleus was the most important determinant of septum position. His findings are complicated by a number of anomalous results, however. The most interesting of these in the present context is illustrated in figure 24. Large nuclei, probably fused daughter nuclei from the previous division, were sometimes found trapped in a centrally located but incomplete division septum (figure 24*a*). At the next division, two new septa were initiated, in some cases located halfway between the existing septum and the end walls (figure 24*b*). This suggests that cells may have the ability to bisect their length regardless of nuclear position, using existing septa and end walls as reference points.

While without repetition and reinterpretation the *Spirogyra* experiment cited is merely suggestive, the evidence against control by the nucleus or other obvious cytoplasmic organelles is much clearer for desmids. By various experimental means, double cells with two isthmuses, but only one nucleus, can be produced (figure 25*a*). At mitosis, septa develop at both isthmuses (figure 25*b*). Judged by the ability of the three cells thus formed to at least begin normal morphogenesis (the anucleate cell eventually arrests), there can be little doubt that the girdle and septum at the anucleate isthmus are normally constructed. Normal septa are also formed even when the nucleus is entirely displaced from the isthmus by antimicrotubule agents (Lehtonen 1977). Septum position is not therefore a consequence of nuclear position in desmids nor, by experimental means, has any more likely governing influence been identified.

PHILOSOPHICAL TRANSACTIONS OF THE ROYAL SOCIETY B BIOLOGICAL SCIENCES

(iii) *Branching patterns*

A dichotomous branch corresponding with the J_{21} pattern has been suggested above as appropriate for *Micrasterias*, in which two lateral wings and twofold symmetry is the normal condition. For Tyson's Brusselator, the importance of symmetry features of the system as a whole in selecting and orienting a particular pattern mode from a range of competing modes has been repeatedly stressed (§3.3). The correct reproduction of twofold semicell symmetry in

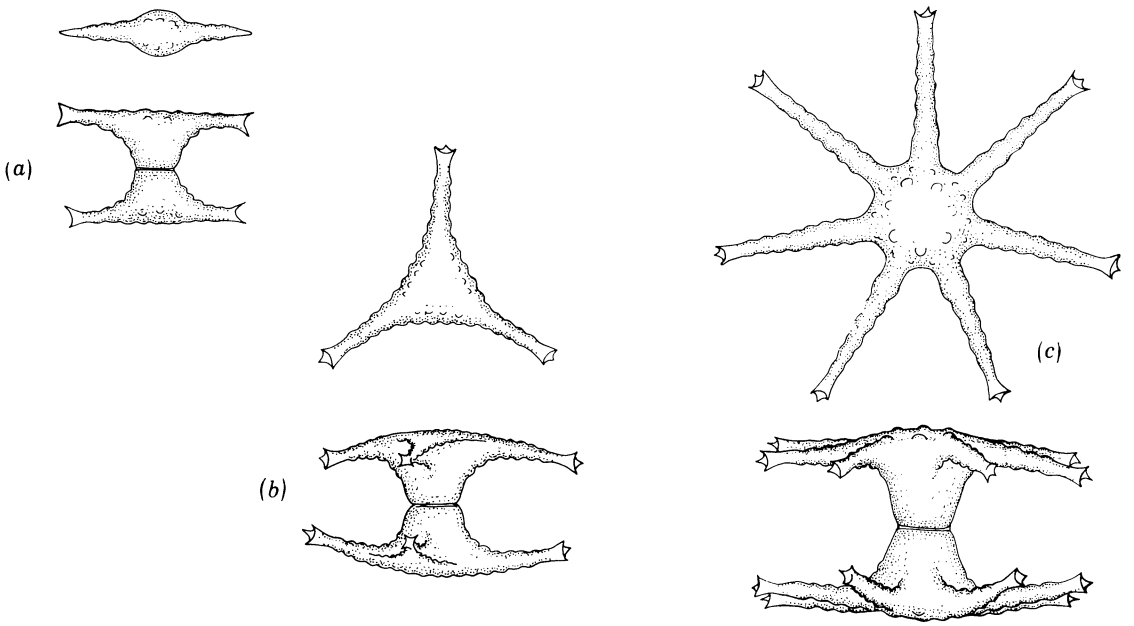

FIGURE 26. Vegetative cell morphology in *Staurastrum*. (*a*) *S. duacense*, (*b*) *S. sebaldi* and (*c*) *S. ophiura*. From West & West (1923, vol. 5). (Magn. × 350.)

Micrasterias after each division is then not surprising if some means exists whereby the parent semicell can bias this selection process in favour of its own symmetry. What remains mysterious is the mechanism by which this is accomplished. The simplest possibility, that isthmus and septum shape determine the pattern, has the following problem: some species do have an isthmus that is roughly oval, with twofold symmetry, but branching occurs across the short axis (Lacalli 1976) rather than the long axis as predicted for Tyson's model (figure 14).

Aberrant forms of *Micrasterias* with three or four wings per semicell arranged to give three- or fourfold symmetry have been isolated and maintained in culture (Waris & Kallio 1964). Such cells are usually diploid whereas the normal vegetative cell is haploid. If one assumes that isthmus size is unchanged, this combined symmetry and ploidy change is consistent with the size dependence of the corresponding pattern modes. The twofold pattern, J_{21}, should dominate over a size range of from 1.2 to $1.8r_m$ (from figure 11). If doubled nuclear ploidy results in doubled rate constants, any spacing governed by a reaction–diffusion mechanism will, by equation (2) in §8, be reduced by a factor of $2^{-\frac{1}{2}}$. The isthmus is thus made effectively larger, its new size range being from 1.7 to $2.5r_m$, a range dominated for the most part in figure 11 by J_{31} and J_{41}. For a new semicell symmetry to be established, this change in most-favoured pattern mode must presumably win out over the influence of the parent semicell, which would favour the existing symmetry. Once established, maintenance of the new pattern might be

much easier. The existence of uniradiate clones of *Micrasterias*, with a single lateral wing and thus onefold symmetry, is not easily explained by Tyson's model. The corresponding pattern mode, J_{11}, was never observed in computations, and it is difficult to envisage how it might be generated.

Other genera, in their normal morphology, show a wider range of symmetry types than does *Micrasterias*. *Staurastrum* has perhaps the widest; cells have been recorded with between two and eleven radially projecting spines, and a corresponding two- to elevenfold symmetry. Species with predominantly twofold symmetry are known (figure 26*a*). More commonly, species have threefold symmetry (figure 26*b*) or variable symmetry within a restricted range. For example, the species illustrated in figure 26*c* has variable numbers of spines within the range of four to nine. These branching patterns can all be produced by means of Tyson's Brusselator, and it may be significant that patterns with a single ring of more than 12 peaks, which cannot be produced in computations, are also not found in *Staurastrum*.

Repeated terminal branching of semicell lobes and spines is observed during the later stages of cell morphogenesis, and this is conceivably also due to the action of a reaction–diffusion mechanism. In such secondary branching processes, the morphogenetically active area becomes reduced to only the tips of the branching lobes and spines. Secondary branching will not be dealt with here because an adequate theoretical treatment would require a detailed reconsideration of the problem of boundaries and boundary conditions, but the involvement of pattern changes like that shown in figure 15 is clearly a possibility.

(iv) *Wall ingrowth versus outgrowth*

The developmental sequence in figure 21 is intended to deal satisfactorily with pattern specification whether the consequence is an ingrowth or outgrowth. Both types of growth involve localized cell wall deposition. The significant difference between them is that ingrowths (e.g. the septum) are plate- or fold-like, presumably the consequence of a linear growth site maintained at the leading edge, while outgrowths are spine- or lobe-like and thus arise from a radially symmetric or point growth site. The author knows of no exceptions to this generalization in the desmids.

A most striking feature of desmid development is that the same region of the developing semicell can produce ingrowths or outgrowths depending on species and conditions. Thus, for example, the establishment of a girdle and septum as shown in figure 25 is a general feature of cytokinesis in all placcoderm desmids so far examined. During conjugation, an identical girdle is formed at the isthmus, followed by outgrowth of a lobe-like conjugation papilla (figure 27). Because of the size of the papilla, it is difficult to determine the exact site at which growth is initiated, but, to judge from the position at which growth is maximal, a site at or near the midpoint of the girdle is quite reasonable. What is normally a linear growth site is therefore converted, during conjugation, to point growth. The converse can be illustrated by comparing the filamentous desmid *Bambusina* (figure 28) with the solitary species so far mentioned. While in *Micrasterias* and *Staurastrum* the primary branch generates a ring of spines or lobes, in *Bambusina* a ring-shaped ingrowth develops at a corresponding site on the completed septum (figure 28*a*). This allows the daughter cells to telescope out as they expand following deposition of the secondary wall layer (figure 28*b*). In other filamentous forms (e.g. *Desmidium*), two or three similar, but smaller, ingrowing rings form at points corresponding with the sites of outgrowths in non-filamentous genera with two- and threefold symmetry.

PHILOSOPHICAL TRANSACTIONS OF THE ROYAL SOCIETY B BIOLOGICAL SCIENCES

While Tyson's Brusselator will generate both linear and point growth sites (i.e. rings and peaks respectively), it does not appear that the controlling factors in computations, symmetry and boundary conditions, bear much relation to the apparent controlling factor in the biological situation, whether growth is inward or outward. To assess the success of the model, there are some situations in which the tendency to peaks is too great, as in its failure to generate an evenly

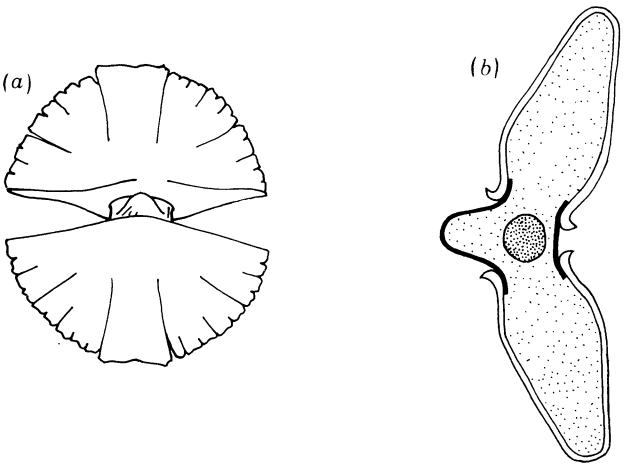

FIGURE 27. Formation of the conjugation papilla in *Micrasterias* seen (*a*) externally and (*b*) in section. After Kies (1973*a*).

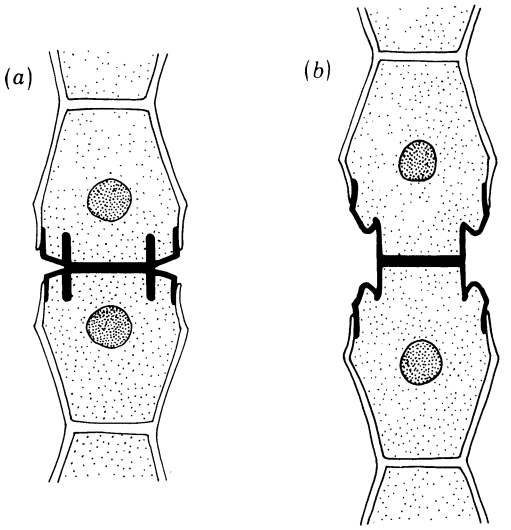

FIGURE 28. Cell expansion following division and septum formation in *Bambusina*, the new wall shown as a heavy line. After Gerrath (1968) and Pickett-Heaps (1975).

ingrowing septum (figure 23). In other situations, a pattern of peaks is too little favoured over the ring, thus making it difficult to obtain two and three peaks on a circular disc despite the common occurrence of this pattern in various desmid genera. There are two ways of adjusting the theory to deal with these discrepancies. (1) A given pattern may be supposed to be due to the action of a single patterning mechanism, but one operating differently depending on whether an ingrowth or an outgrowth is to be produced. The basic mechanism might be assumed, for example, to be similar to Tyson's Brusselator, but with greater tendency to produce

PHILOSOPHICAL TRANSACTIONS OF THE ROYAL SOCIETY B BIOLOGICAL SCIENCES

linear pattern modes. When the wall is not expanding, these patterns would be expressed, and wall deposition along the linear growth site would result. With wall expansion, perhaps with greater turgor, additional features introduced into the mechanism by this change would destabilize or suppress the linear modes in favour of separate peaks. (2) Alternatively, there could be two pattern models operating throughout, one to give linear modes, the second to give a one-dimensional spacing of peaks along these. Harrison *et al.* (1981) use this approach in dealing with pattern in *Acetabularia* (§5). It has the advantage that no limit is placed on the number of peaks that can develop on a ring.

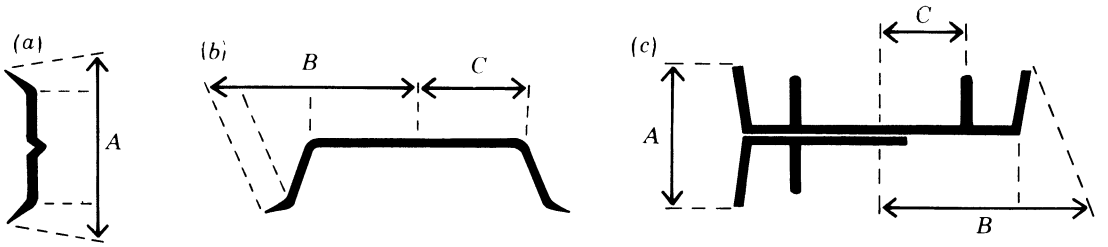

FIGURE 29. Septum dimensions as reported in table 1 for (*a*), (*b*) *Micrasterias* and *Cosmarium* and (*c*) *Bambusina*.

TABLE 1. SEPTUM DIMENSIONS

	$2B/A$	C/B	$\lambda_m/\mu m$	source of data
prediction	3.34	0.45–0.58		
Cosmarium botrytis	3.6	—	13.1	Pickett-Heaps 1972
Micrasterias rotata	3.5	0.57	30.0	Lacalli 1973, 1975*a*
Bambusina brebissonii	3.54	0.49	11.1	Gerrath 1968

4.3. *Quantitative predictions*

Quantitative predictions based on Tyson's Brusselator are compared with published information on desmid morphogenesis in tables 1 and 2.

Table 1 deals with the relative proportions of the girdle and septum, and with the positioning of structures associated with the primary branch. Measurements on three species give very similar results which, within error, agree with predictions. From figure 11, based on linear patterns, the expected ratio can be computed between the maximum diameter of circular disc on which J_{01} pattern can be maintained (taken as the point where the J_{01} curve crosses J_{02}), and the minimum size in one dimension for maintenance of ternary pattern. This is compared in the first column of table 1 with the measured ratio of septum plus girdle diameter at septum completion to girdle width at septum initiation ($2B/A$ as shown in figure 29). The estimated error in the measurements is on the order of 10%. *Bambusina* probably gives the most reliable data. Since there is no cell expansion until secondary wall deposition is well advanced in *Bambusina*, there is no need for measurements to be made at particular developmental stages. For the rings and circles of peaks generated by branching on a disc, a range of values for the ratio of their radius to the radius of the disc obtained from linear patterns and nonlinear computations is given in the second column of table 1. This is compared with the ratio of the distance of the sites of morphogenetic activity on the septum from its centre to the radius of septum plus girdle (C/B in figure 29). For *Micrasterias*, C is measured to the sites of lobe outgrowth as determined by laser experiments (Lacalli 1975*a*). For *Bambusina*, C is measured to the site of

the ingrowth. The value of λ_m, in the third column, is calculated from isthmus diameter. If girdle plus septum radius is taken as $1.36r_m$ as an upperbound, isthmus diameter works out to $1.2\lambda_m$. Observed C/B values support the choice of zero-flux over fixed concentration boundary conditions for models of septum pattern. Morphogen maxima lie much closer to the boundary in the latter case, at least for the assumption of boundary concentrations near the steady state (e.g. $C/B \approx 0.75$–0.9 in Harrison *et al.* (1981)).

Table 2. Ratios of interspine distance to isthmus diameter

	ratio	$\lambda_m/\mu m$	source of data
prediction	0.71	—	—
Cosmarium botrytis	1.0	12.1	Brandham 1965, fig. 17
C. botrytis	1.0	13.3	Berliner & Guth 1979, fig. 5
C. turpinii	1.0	12.1	Starr 1958, fig. 19
Staurastrum denticulatum	1.23	10.8	Brandham 1965, fig. 24
S. furcigerum	1.0	11.5	Pickett-Heaps 1975, fig. 6.169
Euastrum verrucosum	1.17	12.2	Kies 1973*b*, fig. 16
Micrasterias papillifera	1.27	12.6	Kies 1972, figs 3, 4
M. papillifera	1.25	16.5	Coesel & Teixeira 1974, fig. 3

Although the physiological condition of the cell during conjugation is quite different from at mitosis, a relation might be expected between isthmus diameter ($1.2\lambda_m$) and interspine distance on the zygospore ($0.85\lambda_m$ from §3.2). The predicted ratio of spine spacing to isthmus diameter is then 0.71. Table 2 lists observed values of this ratio for six species from four genera. In all cases the observed ratio is larger than expected, that is, spines are too far apart by factors of between 1.4 and 1.8. An interpretation of this, following equation (2) in §8, is that rate constants in the zygospore are between 2 and 3.25 times smaller than in vegetative cells. Despite the discrepancy between prediction and observation, the narrow range of observed ratios among quite different genera is an indication that a common patterning mechanism may be involved in development of both semicells and zygospores.

In summary, Tyson's Brusselator accounts in a general terms for the basic morphogenetic patterns in desmids in that it generates hexagonal arrays and branching patterns of various types with required size dependence. While the model has some unsatisfactory features with regard to semicell pattern (e.g. too great a tendency to give peaks to account for septum initiation), there remain consistent regularities in desmid proportion and patterning that require explanation. These are as yet unexplained except by reaction–diffusion theory.

5. *Acetabularia*

Acetabularia cells are remarkable in size; the nucleus is located at the attached base of the cell, and from this arises a stalk that may be several centimetres in length. The stalk elongates by growth at its tip, which periodically flattens and produces a whorl of hair initials (figure 30). These then elongate and branch. As the cell matures, a final whorl of initials is produced from which the reproductive cap develops. In most species, this last whorl has more initials than previous whorls, and these fuse as they grow to form the rays of the disc-shaped cap. All of the whorls involved in this morphogenetic sequence, whether of hairs or cap rays, appear to have a very regular spacing of pattern elements. Only the hairs are discussed here. They have

PHILOSOPHICAL TRANSACTIONS OF THE ROYAL SOCIETY B BIOLOGICAL SCIENCES

been the subject of extensive study by Harrison *et al.* (1981) and appear, because of greater variability in number, to be more suitable for pattern analysis than are cap rays.

Comparatively few scanning micrographs are available of the early stages of hair formation, but all those examined by the author show spacing between hair initials that is too regular to be accounted for by an inhibitory field mechanism. For example, $R_1 = 1.82$ in the micrograph from which figure 30 is taken. More examples are needed to confirm this result, however.

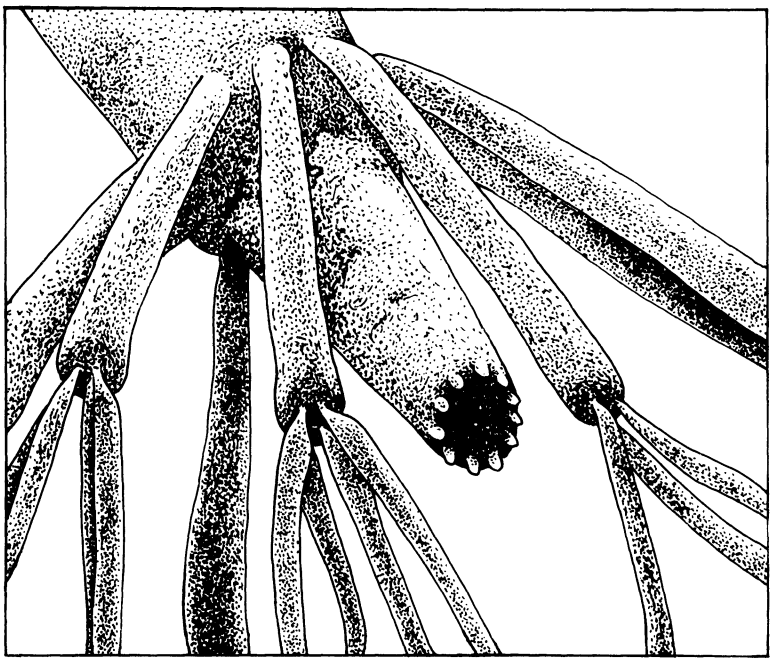

FIGURE 30. An early stage in the development of a whorl of hairs by *Acetabularia major*. From a scanning micrograph supplied by S. Berger also published as fig. 3, pl. 1, in Berger *et al.* (1974). (Magn. × 120.)

Values for the average spacing between hair initials can be calculated from counts of hair number and measurements of tip diameter at the time the initials first appear. A large sample of such measurements has been compiled for *A. mediterranea* (Harrison *et al.* 1981), which show constant spacing over a range of tip sizes (i.e. larger tips have more hairs) with spacings on the order of 20 μm at 20 °C and a well defined dependence of spacing on temperature within a range of about 20 ± 5 μm. Pattern scale is thus very similar to that seen in desmids (§4.3).

The regularity and constancy of the spacing of hair initials strongly suggest the possibility of pattern control by a reaction–diffusion mechanism. The conversion of the site of morphogenetic 'action' during hair formation from a central point (during tip growth) to a ring (flattening) and then to a ring of points (hair initials) clearly parallels the computed pattern changes discussed in §3.3, and is evidence for the involvement of a mechanism like Tyson's Brusselator. One important difference is, however, that *Acetabularia* produces significantly more initials than the computed patterns have peaks. Harrison *et al.* (1981) resolve this problem by suggesting that two Turing models may be needed, one of the Brusselator-type to produce the ring, and a second to give repeated pattern in one dimension around the circumference of the ring, with the number of peaks proportional to circumference. The second model therefore needs λ_m dependent on cues from the first, for example, small λ_m where concentration maxima are generated by the first model (around the ring) to give multiple peaks and large λ_m elsewhere so

that no other peaks form. The concentration dependence required of λ_m to achieve this can be introduced into the parameters of Turing-type models in various ways. Harrison & Lacalli (1978) discuss one example of how this might be done.

6. Diatom patterns

Although there is an extensive literature on valve morphology of diatoms, the development of form in these elaborate structures has been documented in only a few cases. Following cell division, each daughter forms a silicalemma, a flattened, membrane-bound structure lying just

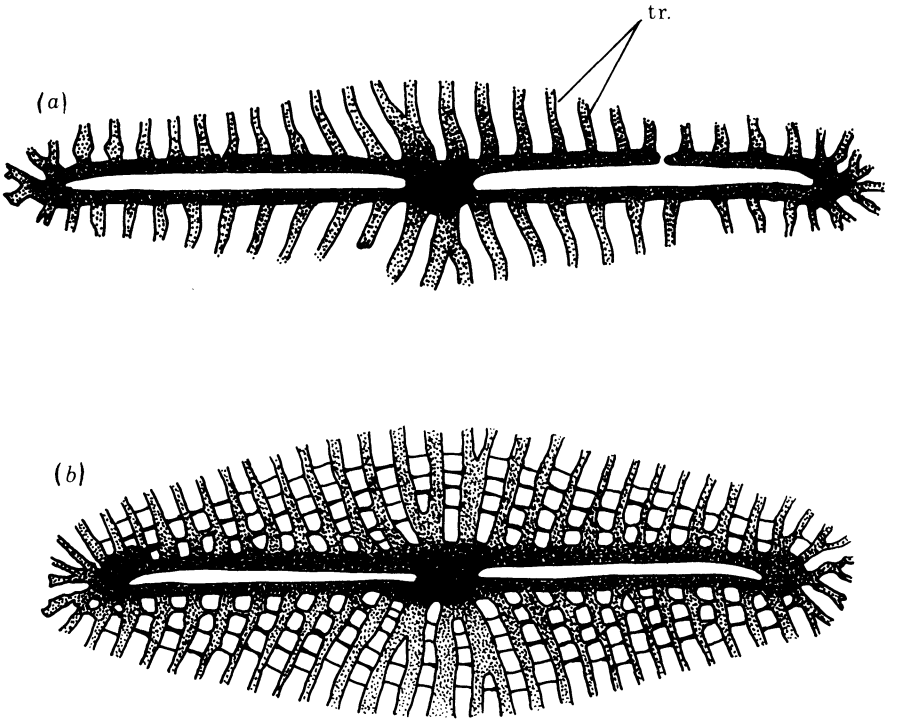

Figure 31. Developing valves isolated from the pennate diatom *Navicula pelliculosa* showing (*a*) an early stage (magn. ×20000) and (*b*) a later stage with cross-bridges forming between the transapical ribs (tr.) (magn. ×16000). From figs 4*a* and 5*a* of Chiappino & Volcani (1977).

beneath the membranes dividing the two cells. Silica is then deposited within this to form the new valve. Certain features of valve morphology appear to depend upon the ordering of cytoplasmic structures (e.g. the shape of the raphe according to Pickett-Heaps *et al.* 1979), but a number of periodic patterns develop as part of valve morphogenesis that cannot be explained in this way. In terms of pattern scale, these differ from spacings in desmids and *Acetabularia* by almost two orders of magnitude, but otherwise show many similar pattern features. Figure 31 shows two stages in the outgrowth of transapical ribs in the pennate diatom *Navicula*. Growth is by addition at the tips of the ribs, which appear irregular in the figure because the newly deposited tip material is partly eroded by the preparatory techniques used. The pattern in figure 31 of interest in the present context is the very regular spacing of ribs along the axial raphe. For ribs along one side in each of figure 31*a*, *b*, R_1 equals 1.88 and 1.90 respectively, with spacings of about 0.25 μm. In addition, dichotomous branching is involved in maintaining

PHILOSOPHICAL TRANSACTIONS OF THE ROYAL SOCIETY B BIOLOGICAL SCIENCES

the regular spacing wherever the ribs diverge as a result of their growth. Branching is more clearly seen in centric diatoms (figure 32*a*), where radial outgrowth from the centre (Schmid & Schulz 1979) results in much greater divergence and branching. These patterns are most readily interpreted as two-dimensional consequences of a one-dimensional spacing mechanism operating along the growing edge. The patterns constitute a record over time of the adjustments that the growth sites responsible for the ribs have made relative to one another.

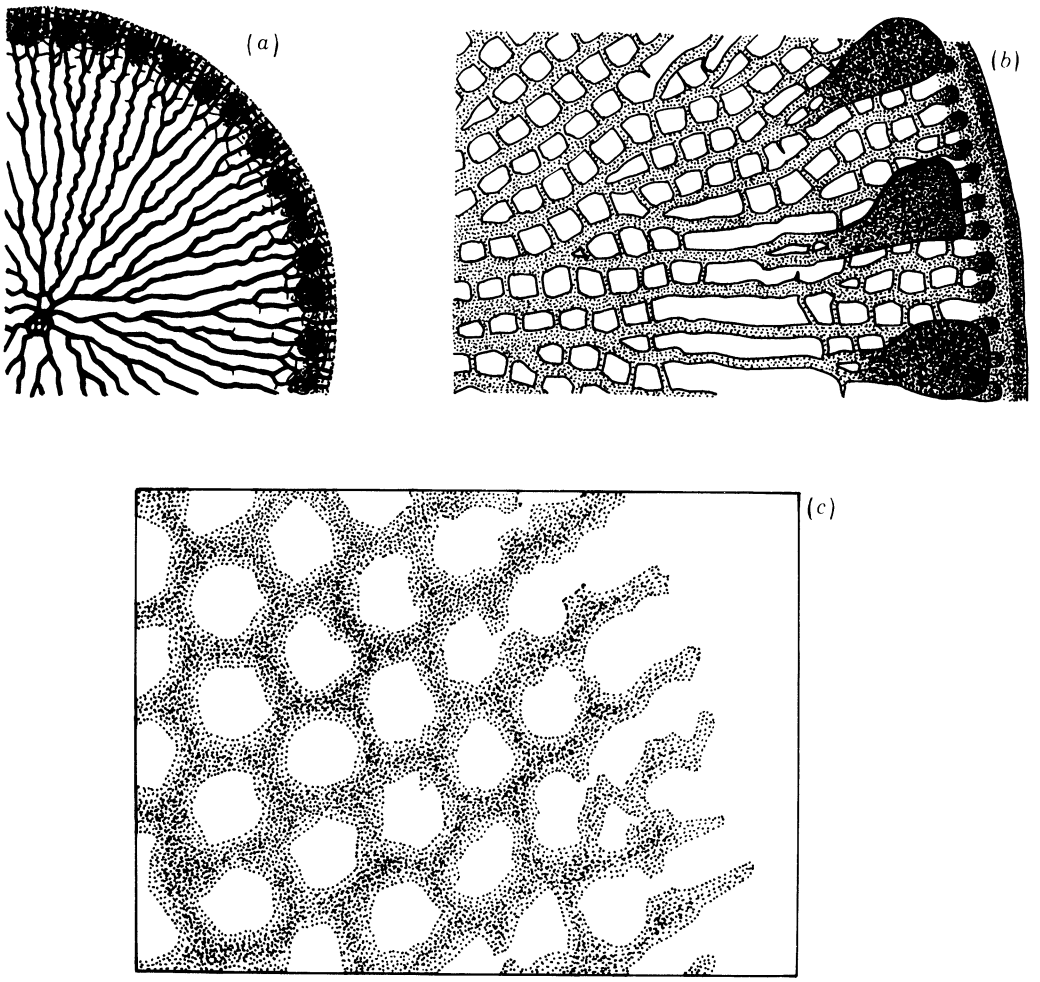

FIGURE 32. Frustule morphology of selected centric diatoms. (*a*) *Detonula confervacea* (magn. ×6000) and (*b*) *Detonula pumila* (magn. ×12000). From figs 60 and 71 of Hasle (1973). (*c*) *Thalassiosira eccentrica*, the edge of the growing valve during development (magn. ×15000). From an unpublished scanning micrograph of an isolated valve supplied by A. M. Schmid.

A second type of periodic pattern, a regular array of hexagonal cells resembling a honeycomb, is characteristic of many centric diatoms (see, for example, Hasle 1973). The initial pattern of silica deposition in these cases (figure 32*c*) is essentially the reverse of the hexagonal pattern seen in desmid zygospores, corresponding to the valleys in computed X morphogen distributions (in figure 9*a*) rather than to the peaks.

A comparison of different parts of the same valve in some species and between valves in related species frequently shows regions of transition between the two types of pattern just described, from radial ribs (figure 32*a*), to ribs with cross-bridges (figures 31*b*, 32*b*), to honey-

comb patterns of varying degrees of regularity (figure 32*b*; see Hasle (1973) for additional examples). This represents a transition from a situation in which the most obvious periodicity is along the one-dimensional edge of a two-dimensional structure to one in which the two-dimensional surface of the structure is itself highly ordered. Although Tyson's Brusselator can generate both patterns separately, it is not clear whether it can be expected to produce the two in turn. This is because the peak that usually branches in one dimension, the *X* peak, ends up

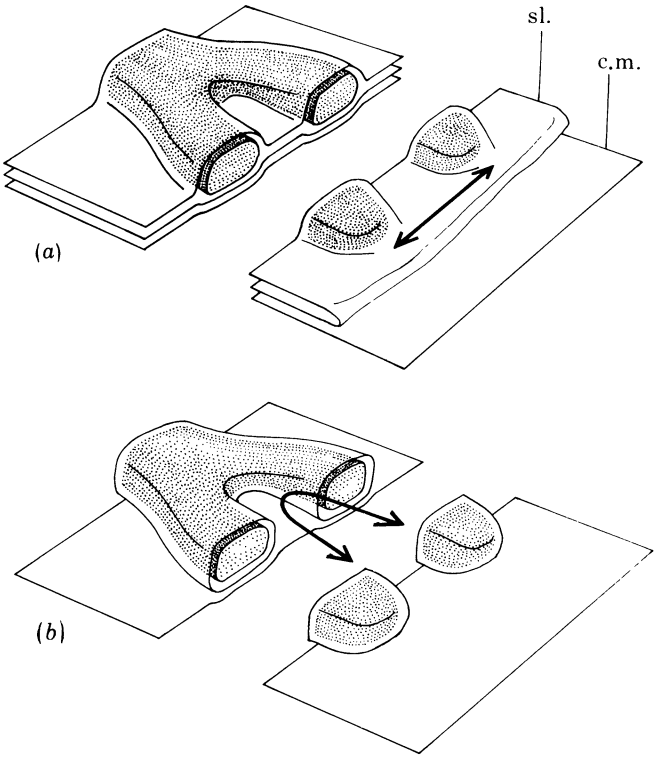

FIGURE 33. Two possible ways the silicalemma (sl.) may invest pattern elements of the developing valve, shown here as a bifurcating rib. (*a*) The silicalemma is continuous between adjacent ribs so that distance can be measured directly across intervening membrane (arrow). (*b*) The silicalemma conforms to the outline of the ribs so that distance between adjacent ribs can be measured directly across intervening cytoplasm or cell membrane (c.m.), but only indirectly (curved arrow) along the silicalemma.

as a peak rather than a valley in two dimensions. The pattern sequence could conceivably be generated by Tyson's model if deposition were to occur in regions with high concentrations of the Y morphogen, since *Y*, out of phase with *X*, is at a maximum along the valleys in the hexagonal pattern, and, also, the pattern change in one dimension for the special case of low k_g values (as in figure 3) would produce a dichotomous branch in all *Y* maxima. Other reaction–diffusion models may be found, however, that give patterns corresponding with those seen in diatoms without requiring the additional assumptions of low k_g and Y, which has very broad concentration peaks, as the significant morphogen.

The complex arrangement of membranes around the developing valve deserves some comment because of the role membrane may play in morphogenesis. The valve is composed of amorphous silica, and R. Gordon of the University of Manitoba (personal communication) has developed a model for pattern based on the solidification properties of the silica itself. An alternative approach, adopted here, is to suppose that morphogenesis is a matter of where,

PHILOSOPHICAL TRANSACTIONS OF THE ROYAL SOCIETY B BIOLOGICAL SCIENCES

within the silicalemma, the deposition of silica is allowed to occur. The membrane of the silicalemma then becomes a prime candidate as a site of pattern formation. In the pennate diatoms so far studied, the silicalemma is a pancake-like structure whose outer edge is smooth rather than conforming to the outline of the developing ribs, as is shown in figure 33*a* (J. D. Pickett-Heaps, A. M. Schmid, personal communication). In any interactions between adjacent ribs involving the membrane, the effective distance between the ribs then corresponds simply to the linear distance between their tips as shown, and the generation of one-dimensional periodicity at the growing edge is quite reasonable. In the one centric diatom so far studied in this regard (*Thalassiosira eccentrica*, figure 32*c*), the edge of the silicalemma appears to conform to the outline of the growing valve as in figure 33*b* (A. M. Schmid, personal communication), so that direct measurement of the distance between adjacent ribs would have to be across the cytoplasm. As an alternative, pattern could be laid out in advance in two dimensions in the adjacent cell membrane, and growth of the silicalemma and valve simply follow this as a template. This may explain why the silicalemma might conform to the outline of the valves in species with hexagonal patterns, but not in *Navicula*, since the latter requires that pattern be generated as the valve grows, while the former may not.

7. Conclusions and suggestions for further work

The analysis of pattern in the foregoing sections falls far short of proving that a reaction–diffusion mechanism is responsible for algal morphogenesis. The author's intent in cataloguing and correlating observed and computed patterns is, rather, to suggest a phenomenological framework for pattern formation, essentially a set of developmental rules, to serve as a basis for further study. To collect more and better pattern correlations is clearly one way to verify and refine such a framework, but an experimental approach is also possible. A common strategy in experimental work on pattern has been to identify those elements of cell structure that are required for pattern formation by testing whether, if they are damaged or destroyed, the pattern is also destroyed. A better experiment is one that leaves the pattern intact, but alters some pattern parameter in a way that can be quantified and interpreted. Within the context of reaction–diffusion theory, pattern spacing is one parameter suitable for this kind of approach.

For reaction–diffusion models in general, the expression for spacing is of the form

$$\lambda_{\mathrm{m}} = 2\pi(\mathscr{D}/k)^{\frac{1}{2}}, \tag{2}$$

where $\mathscr{D}$ and k represent various combinations of diffusivities and rate constants depending on the particular model. For correct dimensionality, k must behave as a first order rate constant. Values for k can then be determined if $\mathscr{D}$ and λ_{m} are known or can be estimated. For the observed spacing in desmids and *Acetabularia*, if diffusion is assumed to occur in the cell membrane (maximum $\mathscr{D} \approx 10^{-8}$ cm^2/s), k will be of the order of 0.1 s^{-1}. For diffusion in an aqueous medium (maximum $\mathscr{D} \approx 10^{-5}$ cm^2/s), k is 10^2 s^{-1}. If k is assumed to be temperature dependent in the usual exponential fashion, $k = A \exp(-E_k/RT)$, and the magnitude of the pre-exponential factor is roughly that of a typical first order chemical reaction ($A \approx 10^{12}$ s^{-1}), an expected value for the activation energy (E_k) can be calculated. Under these assumptions, E_k is 18 kcal/mol (75 kJ/mol) for diffusion in a membrane and 14 kcal/mol (58 kJ/mol) for aqueous diffusion. Both values are within a range that is reasonable for a first order reaction. Harrison *et al.* (1981) have developed their analysis of spacing further by examining the tem-

perature dependence of equation (2), assuming similar exponential form for $\mathscr{D}$ and k. Using *Acetabularia*, they show the logarithm of spacing to vary with reciprocal temperature in good agreement with prediction and confirm the E_k values just given. This type of analysis shows considerable promise as a means of investigating the physicochemical basis of pattern formation in detail.

For Tyson's model, k in equation (2) is replaced by $(a^2c/d)^{\frac{1}{2}}$ multiplied by a constant (§8.2). If the model is accepted as, at least, a formal representation of reality, the rate constants in this expression could still conceal considerable mechanistic complexity. Interpretation of the model is, however, simplified by the involvement, in pattern formation, of a two-dimensional surface in contact with a three-dimensional cytoplasmic reservoir. The formation step in the model represents the appearance of Y in the system of interest, the cell surface. This may be by transfer of Y from the cytoplasm rather than actual Y synthesis. The destruction step likewise corresponds to loss of X from the system of interest whether or not actual degradation is involved. These transfer reactions are likely to be mechanistically quite simple in comparison with the chains of reactions usually involved in biosynthetic events. There is therefore some promise that further study of the magnitude and behaviour of k will yield useful information regarding underlying reaction mechanisms.

Equation (2) is potentially of great importance with regard to identifying the site of pattern formation. If pattern were generated in the cell membrane, any alteration of membrane fluidity would affect spacing in a predictable way by changing $\mathscr{D}$. It would therefore be useful to examine the effect on spacing of physical or chemical treatments known to alter membrane fluidity (e.g. cause phase transitions) as an indication of the involvement of the membrane in pattern formation. Further, simply because diffusion occurs at such different rates in membrane and in aqueous solutions, even crude measurements of the time scale of pattern formation might indicate which of these two phases is involved. Since diffusivities are of the order of 10^3 times smaller in membrane than in aqueous systems, 10^3 times longer is required for a given pattern to develop or change in the membrane than in the cytoplasm or cell wall, if one assumes that diffusion in the latter two is not impeded in some unexpected way. By way of illustration: if the computations based on Tyson's Brusselator are scaled in size to match observed patterns in desmids and *Acetabularia* (§8.2), typical values for membrane diffusivities give a time scale of 0.67 s per computational iteration (i.e. 1000 iterations $\approx$ 11 min). The time required for pattern to develop from the uniform steady state in computations depends to a considerable extent on the fluctuation size used, but appears to require of the order of 10^4 iterations as a minimum (see, for example, figures 1 and 7). The time required for established patterns to change and stabilize in response to growth similarly depends on how rapidly system size is changed in the computations, but a few thousand iterations are needed in most cases. This translates to a few tens of minutes in real time if diffusion is in the membrane. For aqueous diffusion, the time scale is 6.7×10^{-4} s per iteration, and equivalent pattern changes would take only a few seconds. Morphogenesis in desmids and *Acetabularia* occurs over periods of several hours in most instances. Pattern changes taking of the order of tens of minutes are therefore a possibility, but are clearly near the limit of time available. In the event that further observation shows patterns to change much more rapidly, the involvement of membrane in pattern formation could well be ruled out.

PHILOSOPHICAL TRANSACTIONS OF THE ROYAL SOCIETY B BIOLOGICAL SCIENCES

8. Mathematical and computational details

8.1. *Choice of parameter values*

The conditions under which changes in parameters lead to changes in pattern behaviour for two-morphogen Turing models are discussed by Lacalli & Harrison (1979) in terms of three rate parameters, k_1' and k_4', and n, the ratio of diffusivities ($=\mathscr{D}_Y/\mathscr{D}_X$).

For Tyson's Brusselator:

$$k_1' = \left(\frac{d}{2a^2c}\right)^{\frac{1}{2}} \frac{d(a^2c - bd^2)}{(a^2c + bd^2)}, \tag{3}$$

$$k_4' = -\left(\frac{d}{2a^2c}\right)^{\frac{1}{2}} \frac{(a^2c + bd^2)}{d^2}. \tag{4}$$

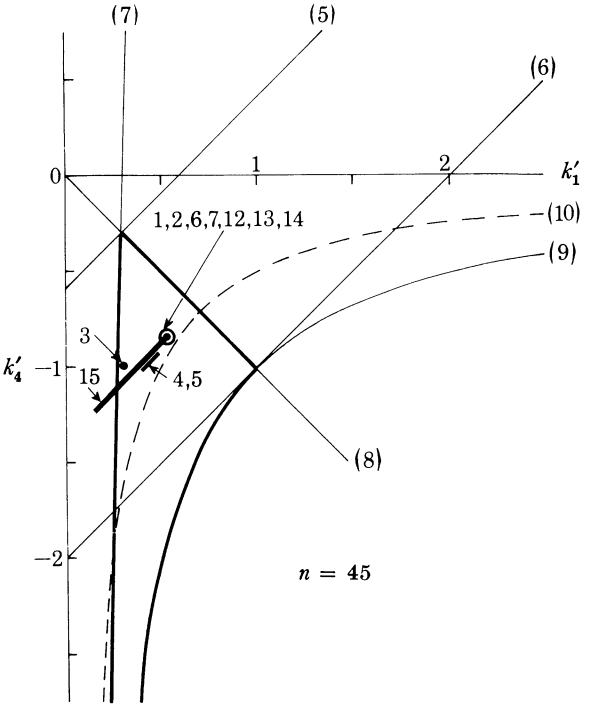

Figure 34. Turing's conditions on parameters in terms of k_1' and k_4' for $n = 45$. Numbering of lines (in parentheses) corresponds with the numbering of equations in the text. Numbers without parentheses refer to the figures in which the parameter values indicated are used.

Significant boundaries in parameter space are defined by the following relations:

$$k_1' - k_4' = 4n^{\frac{1}{2}}/(n+1); \tag{5}$$

$$k_1' - k_4' = 2; \tag{6}$$

$$nk_1' - k_4' = 2n^{\frac{1}{2}}; \tag{7}$$

$$k_1' + k_4' = 0; \tag{8}$$

$$k_1'k_4' = -1. \tag{9}$$

Stable spatial patterns are obtained for parameters falling within the region defined by the intersections of (7), (8) and (9), as shown in figure 34. Tyson's Brusselator is restricted to the

region to the left of the dotted line, which is the limit for b decreasing to zero:

$$k_1' k_4' = -\tfrac{1}{2}. \tag{10}$$

The locations of the parameters used in each figure are also shown in figure 34, with the parameter gradients in figures 4, 5 and 15 drawn as heavy lines. The gradients were chosen to give constant λ_m over their full extent. This is facilitated but not guaranteed by having a gradient whose slope is $+1$ in $k_1' k_4'$ space, parallel to (5) and (6). The gradient used in figure 15 crosses line (7). This is the boundary separating regions of positive and negative k_g at λ_m, lying to the right and left, respectively, of (7).

Parameters for individual figures are as follows.

Figure 1: $a = c = 1.06d = 0.00185$, $b = 0.0002$, $\mathscr{D}_X = 0.01$, $n = 40$, $l = 30$. Fluctuations of ± 0.0005 times X concentration were introduced at one array position per iteration. A similar fluctuation size was used in the other computations.

Figure 2: initial parameters as in figure 1, with gradual change to $2k$, $0.5\,\mathscr{D}$; k_g at $\lambda_m = 0.0013$.

Figure 3: initial $a = c = d = 0.0025$, $b = 0.001$, $\mathscr{D}_X = 0.01$, $n = 40$, $l = 30$, with gradual change to $2k$, $0.5\,\mathscr{D}$; k_g at $\lambda_m = 5 \times 10^{-5}$.

Figure 4: initial $a = c = 1.11d = 0.0025$, $b = 0.00068$ at edge to 0.00036 at centre, $\mathscr{D}_X = 0.01$, $n = 40$, $l = 30$, with gradual change to $5k$, $0.5\,\mathscr{D}$.

Figure 5: as in figure 4 with reversed gradient in b.

Figure 6: (a) as in figure 1 but with $l = 20$; (b) gradient in a from 0.00185 at edges to 0.00215 at centre.

Figure 7: $a = c = 1.06d = 0.0148$, $b = 0.0016$, $\mathscr{D}_X = 0.005$, $n = 40$. Intersecting lines in the figure correspond with the centre of the grid squares used in the computation. In all two-dimensional computations, fluctuations were introduced at between 5 and 20 array positions per iteration. For this figure, 20 fluctuations per iteration of 0.0005 times X concentration were used.

Figure 9b: $\rho_0 = 6 \times 10^{-4}$, $\rho = \rho' = 0.4$, $c = 0.05$, $c' = 0.025$, $\mu = 0.21$, $\nu = 0.27$, $\mathscr{D}_a = 0.005$, $\mathscr{D}_h = 0.225$.

Figure 11: as in figure 1.

Figure 12: initial values as in figure 1 but with $\mathscr{D}_X = 0.005$, $n = 20$; k changed to 2, 2.5 and 5 times initial values in (b)–(d) respectively, $r_0 = 12$, $\Delta\theta = \pi/12$.

Figure 13: initial values as in figure 1 but with $\mathscr{D}_X = 0.005$, $n = 45$; k changed to 1.35, 2, 3, 5 and 7 times initial values in (b)–(f) respectively.

Figure 14: as in figure 13 but with $1.35k$ in (a), $2k$ in (b)–(d).

Figure 15: initial $a = c = 1.025d = 0.0123$, $b = 0.001$ at centre to 0.0071 at edges, $\mathscr{D}_X = 0.005$, $n = 45$, changes to $1.65a$, $1.65c$, $1.65d$ and $2.3b$ in (b); $2.45a$, $2.45c$, $2.45d$ and $3.5b$ in (c)–(e).

Figure 23: (a) pattern at 4000 iterations, $c = 1.06d = 0.00555$, a goes from 0.00555 at edges to 0.0065 at centre, $b = 0.0006$, $\mathscr{D}_X = 0.005$, $n = 45$; (b) pattern at 6000 iterations, a goes from 0.0048 at edges to 0.007 at centre, $c = 0.0048$, $d = 0.00525$, $b = 0.0006$, $\mathscr{D}_X = 0.005$, $n = 45$. Boundary conditions in both are zero-flux along the sides and periodic at the ends.

PHILOSOPHICAL TRANSACTIONS OF THE ROYAL SOCIETY B BIOLOGICAL SCIENCES

8.2. *Dependence of spacing on $\mathscr{D}$ and k*

The general equation for λ_m given by Lacalli & Harrison (1978*a*) becomes, for Tyson's Brusselator,

$$\lambda_m^2 = 4\pi^2(\mathscr{D}_Y - \mathscr{D}_X) \Big/ \left\{ \left(\frac{2a^2c}{d}\right)^{\frac{1}{2}} \left[\frac{(n+1)}{n^{\frac{1}{2}}} - k_1' + k_4' \right] \right\}. \quad (11)$$

The expression in brackets in the denominator has narrow limits for reasonable values of n. Within the limits for stable pattern (figure 34), the value of $k_1' - k_4'$ reaches a maximum at the intersection of lines (7) and (10) and a minimum at the intersection of (7) and (8). The coordinates of these points are $(1+2^{\frac{1}{2}})/n^{\frac{1}{2}}$, $n^{\frac{1}{2}}/(2+2^{\frac{1}{2}})$ and $2n^{\frac{1}{2}}/(n+1)$, $-2n^{\frac{1}{2}}/(n+1)$ respectively. The range of possible values for the expression in brackets is then between $(n-1)^2/[n^{\frac{1}{2}}(n+1)]$ and $[(1+2^{\frac{1}{2}})/(2+2^{\frac{1}{2}})]\,[(n-1)/n^{\frac{1}{2}}]$. For large n, these limits can be approximated as $0.7\,n^{\frac{1}{2}}$ and $n^{\frac{1}{2}}$ respectively giving values of 6 ± 4 for a typical range of n from 10 to 100, sufficient to take in molecules of quite different size and properties as long as they are diffusing within the same medium. Taking $n = 25$, since $\mathscr{D}_Y - \mathscr{D}_X \approx \mathscr{D}_Y$ for large n, gives

$$\lambda_m^2 \approx 5\mathscr{D}_Y\,(d/a^2c)^{\frac{1}{2}}. \quad (12)$$

The arbitrary space and time units of the computations are readily converted to real units by means of the above expressions for λ_m. For computations in two dimensions, typical parameters are $a = c = d = 0.01$, $\mathscr{D}_Y = 0.2$, which gives $\lambda_m \approx 10$. Observed spacings (desmids and *Acetabularia*) are of the order of 2×10^{-3} cm. The spatial conversion factor appropriate to these examples is then 2×10^{-4} cm per spatial unit. For diffusion of small molecules in cell membranes, $\mathscr{D} \approx 10^{-8}$ cm^2/s (Poo *et al.* 1979), and the required time factor is then 0.67 s per iteration. For an aqueous system, maximum values for diffusivities are around 10^{-5} cm^2/s, and the time factor is correspondingly smaller: 6.7×10^{-4} s per iteration.

This work was supported by operating grants from the National Research Council (now N.S.E.R.C.) of Canada. I thank L. G. Harrison for stimulating discussions of the morphogenetic theory and A. M. Schmid, S. Berger, J. D. Pickett-Heaps and D. H. Tippit for allowing the use of unpublished results and micrographs. Mr Dan Etcheverry assisted with the computations.

References

Berger, S., Sandakhchiev, L. & Schweiger, H. G. 1974 Fine structural and biochemical markers of Dasycladaceae. *J. Microsc.* **19**, 89–104.

Berliner, M. D. & Guth, E. 1979 Zygote formation in *Cosmarium botrytis*. *Protoplasma* **101**, 1–10.

Brandham, P. E. 1965 Polyploidy in desmids. *Can. J. Bot.* **43**, 405–417.

Bunow, B., Kernevez, J. P., Joly, G. & Thomas, D. 1980 Pattern formation by reaction–diffusion instabilities: application to morphogenesis in *Drosophila*. *J. theor. Biol.* **84**, 629–699.

Chiappino, M. L. & Volcani, B. E. 1977 Studies on the biochemistry and fine structure of silica shell formation in diatoms VII. *Protoplasma* **93**, 205–221.

Claxton, J. H. 1964 The determination of patterns with special reference to that of the central primary skin follicles in sheep. *J. theor. Biol.* **7**, 302–317.

Coesel, P. F. M. & Teixeira, R. M. V. 1974 Notes on sexual reproduction in desmids: II. *Acta bot. neerl.* **23**, 603–611.

Crank, J. 1975 *The mathematics of diffusion* (2nd edn). Oxford: Clarendon Press.

Crowther, R. A., Finch, J. T. & Pearse, B. M. F. 1976 On the structure of coated vesicles. *J. molec. Biol.* **103**, 785–798.

PHILOSOPHICAL TRANSACTIONS OF THE ROYAL SOCIETY B BIOLOGICAL SCIENCES

Erneux, T. & Herschkowitz-Kaufman, M. 1975 Dissipative structures in two dimensions. *Biophys. Chem.* **3**, 345–354.
Erneux, T. & Herschkowitz-Kaufman, M. 1979*a* Bifurcation diagram of a model chemical reaction: I. *Bull. math. Biol.* **41**, 21–38.
Erneux, T. & Herschkowitz-Kaufman, M. 1979*b* Bifurcation diagram of a model chemical reaction: II. *Bull. math. Biol.* **41**, 767–790.
Gerrath, J. F. 1968 Studies on the ultrastructure of desmids and its relation to their taxonomy. Ph.D. thesis, University of British Columbia.
Gierer, A. & Meinhardt, H. 1972 A theory of biological pattern formation. *Kybernetik* **12**, 30–39.
Glansdorff, P. & Prigogine, I. 1973 Equilibrium variation interpreted as a source of order: dissipative structures. *Bull. Acad. r. Belg. Cl. Sci.* **59**, 672–702.
Gmitro, J. I. & Scriven, L. E. 1966 A physicochemical basis for pattern and rhythm. *Symp. int. Soc. Cell Biol.* **5**, 221–255.
Hackstein-Anders, C. 1975 Untersuchungen zur Cytomorphogenese von *Micrasterias* unter Einfluss von Actinomycin D und Ethidiumbromid. *Protoplasma* **86**, 83–105.
Harrison, L. G. & Lacalli, T. C. 1978 Hyperchirality: a mathematically convenient model for the kinetics of morphogenesis. *Proc. R. Soc. Lond.* B **202**, 361–397.
Harrison, L. G., Snell, J., Verdi, R., Vogt, D. E., Zeiss, G. D. & Green, B. R. 1981 Hair morphogenesis in *Acetabularia*: temperature-dependent spacing and models of morphogen waves. *Protoplasma.* **106**, 211–221.
Hasle, G. R. 1973 Some marine plankton genera of the diatom family Thalassiosiraceae. *Nova Hedwigia* **45**, 1–68.
Hepler, P. K. & Fosket, D. E. 1971 The role of microtubules in vessel member differentiation in *Coleus*. *Protoplasma* **72**, 213–236.
Herschkowitz-Kaufman, M. 1975 Bifurcation analysis of nonlinear reaction-diffusion equations: II. *Bull. math. Biol.* **37**, 589–636.
Hertz, P. 1909 Über den gegenseitigen durchschnittlichen Abstand von Punkten. *Math. Annln* **67**, 387–398.
Heslop-Harrison, J. 1968 The emergence of pattern in the cell walls of higher plants. *Devl Biol.* (suppl. 2), 118–150.
Heslop-Harrison, J. 1969 The origin of surface features of the pollen wall of *Tagetes patula* as observed by scanning electron microscopy. *Cytobios* **2**, 177–186.
Heslop-Harrison, J. 1972 Pattern in plant cell walls: Morphogenesis in miniature. *Proc. R. Inst. Gt Br.* **45**, 335–352.
Kauffman, S. A., Shymko, R. & Trabert, K. 1978 Control of sequential compartment formation in *Drosophila*. *Science, N.Y.* **199**, 259–270.
Kiermayer, O. 1970*a* Elektronenmikroskopische Untersuchungen zum Problem der Cytomorphogenese von *Micrasterias denticulata* I. *Protoplasma* **69**, 97–132.
Kiermayer, O. 1970*b* Causal aspects of cytomorphogenesis in *Micrasterias*. *Ann. N.Y. Acad. Sci.* **175**, 686–701.
Kies, L. 1970 Elektronenmikroskopische Untersuchungen uber Bildung und struktur der Zygotenwand bei *Micrasterias papillifera* I. *Protoplasma* **70**, 21–47.
Kies, L. 1972 Geschlechtliche Fortpflanzung von *Micrasterias papillifera*. *Inst. Wiss. Film*, film C 1064/1971.
Kies, L. 1973*a* Elektronenmikroskopische Untersuchungen uber die Konjugation bei *Micrasterias papilliera*. *Nova Hedwigia* **42**, 139–154.
Kies, L. 1973*b* Zygotenbildung bei *Euastrum verrucosum*. *Mitt. Staatsinst. Allg. Bot. Hamburg* **14**, 31–36.
Kubicek, M., Ryzler, V. & Marek, M. 1978 Spatial structures in a reaction–diffusion system: detailed analysis of the 'Brusselator'. *Biophys. Chem.* **8**, 235–246.
Lacalli, T. C. 1973 Cytokinesis in *Micrasterias rotata*. *Protoplasma* **78**, 433–442.
Lacalli, T. C. 1975*a* Morphogenesis in *Micrasterias*: I. *J. Embryol. exp. Morph.* **33**, 95–116.
Lacalli, T. C. 1975*b* Morphogenesis in *Micrasterias*: II. *J. Embryol. exp. Morph.* **33**, 117–127.
Lacalli, T. C. 1976 Morphogenesis in *Micrasterias*: III. *Protoplasma* **88**, 133–147.
Lacalli, T. C. & Harrison, L. G. 1978*a* The regulating capacity of Turing's model for morphogenesis with application to slime moulds. *J. theor. Biol.* **70**, 273–295.
Lacalli, T. C. & Harrison, L. G. 1978*b* Development of ordered arrays of cell wall pores in desmids: a nucleation model. *J. theor. Biol.* **74**, 109–138.
Lacalli, T. C. & Harrison, L. G. 1979 Turing's conditions and the analysis of morphogenetic models. *J. theor. Biol.* **76**, 419–436.
Lehtonen, J. 1977 Morphogenesis in *Micrasterias torreyi* and *M. thomasiana* studied with UV microbeam and chemicals. *Suomal. eläin- ja kasuit. Seur. van. Julk.* **14**, 165–190.
Pickett-Heaps, J. D. 1972 Cell division in *Cosmarium botrytis*. *J. Phycol.* **8**, 343–360.
Pickett-Heaps, J. D. 1973 Cell division and wall structure in *Microspora*. *New Phytol.* **72**, 347–355.
Pickett-Heaps, J. D. 1974 Scanning electron microscopy of some cultured desmids. *Trans. Am. microsc. Soc.* **93**, 1–23.
Pickett-Heaps, J. D. 1975 *Green algae*. Sunderland, Massachusetts: Sinauer.
Pickett-Heaps, J. D., Tippit, D. H. & Andreozzi, J. A. 1979 Cell division in the pennate diatom *Pinnularia*: IV. *Biol. cell.* **35**, 199–206.

PHILOSOPHICAL TRANSACTIONS OF THE ROYAL SOCIETY B BIOLOGICAL SCIENCES

Poo, M. M., Lam, J. W., Orida, N. & Chao, A. W. 1979 Electrophoresis and diffusion in the plane of the cell membrane. *Biophys. J.* **26**, 1–22.
Schmid, A. M. & Schulz, D. 1979 Wall morphogenesis in diatoms: deposition of silica by cytoplasmic vesicles. *Protoplasma* **100**, 267–288.
Selman, G. G. 1966 Experimental evidence for the nuclear control of differentiation in *Micrasterias*. *J. Embryol. exp. Morph.* **16**, 469–485.
Starr, R. C. 1958 The production and inheritance of the triradiate form in *Cosmarium turpinii*. *Am. J. Bot.* **45**, 243–248.
Thompson, D'Arcy W. 1942 *On growth and form* (2nd edn). Cambridge University Press.
Turing, A. M. 1952 The chemical basis of morphogenesis. *Phil. Trans. R. Soc. Lond.* B **237**, 37–72.
Tyson, J. J. & Light, J. C. 1973 Properties of two-component bimolecular and trimolecular chemical reaction systems. *J. chem. Phys.* **59**, 4164–4173.
Tyson, J. J. & Kauffman, S. 1975 Control of mitosis by a continuous biochemical oscillation. *J. math. Biol.* **1**, 289–310.
Van Wisselingh, C. 1909 Zur Physiologie der Spirogyrazelle. *Beih. bot. Zbl.* **24**, 133–210.
Wardlaw, C. W. 1953 A commentary on Turing's diffusion–reaction theory of morphogenesis. *New Phytol.* **52**, 40–47.
Wardlaw, C. W. 1955 Evidence relating to the diffusion–reaction theory of morphogenesis. *New Phytol.* **54**, 39–48.
Waris, H. & Kallio, P. 1964 Morphogenesis in *Micrasterias*. *Adv. Morphogen.* **4**, 45–79.
West, W. & West, G. S. 1904–23 *A monograph of the British Desmidiaceae* (5 vols). London: The Ray Society.

PHILOSOPHICAL TRANSACTIONS OF THE ROYAL SOCIETY B BIOLOGICAL SCIENCES